MARMARA UNIVERSITY
FACULTY OF ENGINEERING

# BIOMIMETIC WIND TURBINE BLADE DESIGN

EGE ENES SATAR, MUSTAFA KAMAK

**GRADUATION PROJECT REPORT**

Department of Mechanical Engineering

**Supervisor**

Doç. Dr. Mustafa YILMAZ

ISTANBUL, 2025

MARMARA UNIVERSITY

FACULTY OF ENGINEERING

**Biomimetic Wind Turbine Blade Design**

**Ege Enes Satar**

**Mustafa KAMAK**

**2025, Istanbul**

**SUBMITTED TO THE DEPARTMENT OF MECHANICAL ENGINEERING IN PARTIAL FULFILLMENT OF THE REQUIREMENTS FOR THE DEGREE**

**OF**

**BACHELOR OF SCIENCE**

**AT**

**MARMARA UNIVERSITY**



Signature of Author(s) **Ege Enes Satar**

**Mustafa KAMAK**

Department of Mechanical Engineering

Certified by **Doç.Dr. Mustafa YILMAZ**

Project Supervisor, Department of Mechanical Engineering

Accepted by **Prof.Dr. Bülent EKİCİ**

Head of the Department of Mechanical Engineering

# ACKNOWLEDGEMENTS

We would like to extend our sincere thanks to our advisor Doç. Dr. Mustafa YILMAZ for enabling the realization of this study. His guidance and advice have directed us at every stage of our thesis. His insights and mentorship have contributed to the development of our critical thinking skills and have improved our methods for solving complex engineering problems. Additionally, we would like to express our gratitude to the committee members for permitting our defence and for their thoughtful comments and suggestions.

# CONTENT

# ABSTRACT

A key element of sustainable power generation is wind energy, and increasing efficiency greatly depends on perfecting the design of wind turbine blades. In order to enhance performance, this study focuses on the biomimetic design of wind turbine blades, taking cues from vulture wing aerodynamics. To improve overall aerodynamic efficiency, raise the lift-to-drag ratio, and decrease induced drag, a bio-inspired winglet was added to the blade design.

The study uses the ANSYS Fluent and Static Structural modules for finite element analysis (FEA) and computational fluid dynamics (CFD). Maximum aerodynamic efficiency was attained through winglet optimization, while mechanical stability was guaranteed through structural analysis. Initially, the winglet utilized Al 7075-T6, leading to an overly high safety factor (FOS = 15). To enhance weight and structural efficiency, alternative materials like Al 6061-T6 and glass fiber reinforced polymer (GFRP) were examined, bringing the safety factor down to an optimal range of 2-3.

The findings indicate that biomimetic winglets significantly reduce induced drag, thereby boosting wind turbine performance. The combination of optimized materials and geometric adjustments offers a balance between structural integrity and weight efficiency, rendering the proposed design practical for real-world applications.

**Keywords:** Biomimetic design, wind turbine blade, winglet optimization, induced drag, CFD, FEA, ANSYS.

# SYMBOLS

$C_L$=Lift Coefficient

$C_D$ =Drag Coefficient

$D_i$ =Induced Drag

$P_r$ = Power generated by turbine

$\rho$ =Density of Air

$A$ =Area swept by the turbine

$V_1$ =Wind Velocity

$C_P$ =Power Coefficient

# ABBREVIATIONS

**NACA =** National Advisory Committee for Aeronautics

**CFD =** Computational Fluid Dynamics

**ABC =** Artificial Bee Colony

**BEM** = Blade Element Momentum Theory

**SF** = Scale Factor

# LIST OF FIGURE

# LIST OF TABLES

# 1.) INTRODUCTION

Wind energy, which is a non-polluting, environmentally friendly and renewable energy source, has become even more important today. Wind turbines, which have an important place in the renewable energy sector, are important components for converting wind energy into mechanical energy through their blades, and their shape designs significantly affect the efficiency of the wind energy generation system. Therefore, efficient capture and use of wind energy to increase energy conversion efficiency are key points in wind turbine blade design. Airfoil design and blade design methods for wind turbines are very important for improving aerodynamic performance. Traditional wind turbine blades have evolved over time, focusing on optimizing aerodynamic performance and durability. However, despite advances in design, traditional turbine blades still face challenges such as efficiency, noise generation and material fatigue.

In recent years, a promising approach to improving wind turbine performance has emerged from nature's own designs. Biomimetic design is the practice of imitating strategies and processes found in biological systems, and this has yielded innovative solutions in a variety of engineering fields, including wind energy. The idea behind biomimetic design is to examine and mimic the forms, structures, and systems that nature has evolved to solve specific challenges; they are often known to provide high efficiency and sustainability.

In this thesis, the application of biomimetic principles in the design of wind turbine blades was investigated. Inspired by the vulture wing, it was aimed to develop a biomimetic wind turbine blade design by investigating the aerodynamic properties of this wing and the properties of the materials that can be used in the wing structure.

## 1.1) History of Wind Turbines

Wind energy has been used for millennia to sail the seas, grind grain, saw timber, press oil, shred tobacco, and pump water. In the late 19th century inventors turned their attention to using the wind for generating electricity. Technological development followed sporadically until the oil crises of the 1970s spurred renewed interest. Since the oil crises of the 1970s and the following Great Wind Revival of the 1980s, wind turbine design has evolved markedly, settling on a characteristic configuration using rotors with three blades, upwind of the tower, in steadily increasing size. Today, modern wind turbines, along with solar photovoltaics, are the principal source of new electricity generating capacity.


*Figure 1 History of Wind Turbines*

## 1.2) What is Biomimetic

"Biomimetic" refers to an approach in technology, design, engineering, and science where inspiration is drawn from nature. This approach aims to understand the functioning of organisms or biological systems in nature and apply that knowledge to create practical applications for humans. Biomimetic design can also be called biomimicry or bio-mimetics. Biomimetic seeks to gain various advantages by taking inspiration from examples in nature. These advantages include developing more efficient and energy-efficient products, sustainability, environmental compatibility, more durable materials, and better functional systems. Over the years, humans have innovated in various fields, such as aircraft wings, water purification systems, drug delivery methods, and more, by drawing inspiration from solutions that organisms in nature have evolved. Biomimicry requires a multidisciplinary approach to understand the workings of nature and integrate this knowledge into technological and design processes. It involves a combination of biology, engineering, chemistry, materials science, and other fields. This approach not only helps in the conservation of the natural world but also contributes to making human-made systems more efficient and environmentally friendly.

# 2.) LITERATURE REVIEW

## 2.1) The use of Biomimetic in Wind Turbines

Biomimetic has been used in the design of wind turbines to enhance their efficiency, reduce environmental impact, and improve their overall performance. Here are some samples in which biomimetic has been applied in wind turbine design:

In the aspect of airfoil research, Rose et al. introduced knowledge and technology from biomimetics and conducted numerical studies on the tubercles inspired by the humpback whale (HW) using a straight wing and a swept-back wing configuration. Metin et al., inspired by biological systems in nature, increased aerodynamic performance by adding small wings and annular blades at the wing tip. Yuan et al. proposed improving the aerodynamic performance of wind turbine blades by refining the trailing edge of the airfoil. Wang et al. proposed a multi-objective optimization model that combines maximizing the power coefficient and minimizing the surface area of the blade for variable pitch wind turbines using a novel airfoil. Wang et al. have established a wind turbine airfoil model based on the Generalized Regression Neural Network (GRNN) and proposed an optimization design method to improve the aerodynamic performance of the airfoil under multiple constraints. Yan et al. , focusing on sturgeons, have conducted numerical simulation studies by employing 3D reverse engineering and B-spline curve fitting techniques to establish physical models of both asymmetric and symmetric biomimetic airfoils. Zhao et al. have designed a novel serrated airfoil inspired by owl wings, enhancing the overall performance of the airfoil. Hua et al. and Lanzafame et al. have also conducted research on airfoil designs. In research on optimization design methods for wind turbine blades, Lee et al. examined various design parameters and utilized the second-order response surface method to establish the correlation between the objective function and factors such as chord length and torsion angle in the design calculations. They compared the performance of the optimized blade with the original design and found significant improvements. Rodriguez et al. proposed an integrated optimization methodology for wind turbine blade design by combining computational fluid dynamics (CFD), blade element momentum theory (BEM), and genetic algorithms (GA). Özkan et al. have developed a novel optimization technique called the Artificial Bee Colony algorithm based on Blade Element Momentum theory (ABC-BEM), which has been applied to designing small-scale wind turbine blades. A, Zhu et al. have proposed a multi-objective optimization design method for wind turbine systems based on a tower-blade coupling model, aiming to explore the coupling effect between the tower and blades to improve the performance of wind turbine systems. Zhu et al. proposed a Matlab-based program combined with Ansys to

achieve an optimal trade-off between maximum power generation and minimum blade mass in wind turbine design. Zemamou et al. investigated the optimization of traditional Savonius blade design using Bézier curves and transient computational fluid dynamics (CFD) simulations. Zhang et al. , Maki et al., Tang et al., among others, have also conducted research on methods for wind turbine blade design.

In depth research has been conducted on the optimization design of wind turbine blades. However, these studies predominantly focus on either airfoil or blade design methods, with limited research on integrating both. This study applies a bionic airfoil design inspired by an eagle, implementing a non-uniform extraction method of blade elements based on the blade element theory for wind turbine blade optimization.

## 2.2) The Effect of the Number of Blades on the Efficiency of a Wind Turbine

Wind turbines extract energy from the wind and convert it into electricity. A wind turbine blade is an important component of a clean energy system because of its ability to capture energy from the wind. The configuration of blades plays an important role in their efficiency. Characteristics such as tip speed ratio, angle of attack, materials used in the manufacture of the wind turbine blade, and weight of the wind turbine blade play important roles in determining the efficiency of blade as well as that of the turbine. In real life, wind turbines cannot capture more than 59.3% of the energy from the wind, which is known as the Betz limit. Blade characteristics determine the amount of energy that can be extracted from the wind. For this reason, improving the performance of a wind turbine blade directly increases the efficiency of the wind power plant. Designers of most commercial wind turbines, which are mostly horizontal axis wind turbines and a few vertical axis wind turbines, have tried to design wind turbines that operate at efficiencies close to the Betz limit. However, there are limitations due to losses in the system from the mechanical assembly in the nacelle. Figure 2 compares the performance of different types of wind turbine to the Betz limit (0.593).

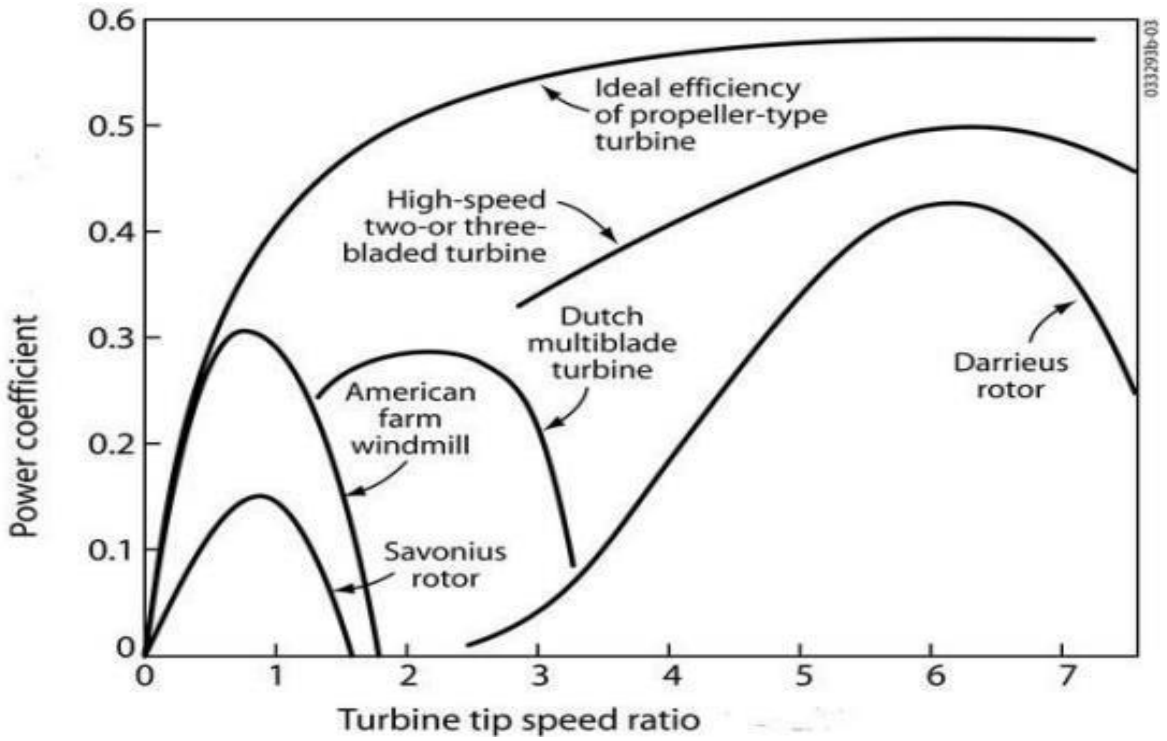


*Figure 2 Comparison between the performances of different types of wind turbine. The Betz limit is 59.3%*

.

Subtracting the sum of the losses from 0.593 gives the maximum amount of energy that can be extracted. According to Siemens in 2007, modern three-blade wind turbines have combined intelligent blade design and a well-chosen rotational speed of up to 80% of the Betz limit. A two-blade turbine will be approximately 5% less efficient that a three-blade turbine, but will provide a higher return on investment due to lower costs. The efficiency of three- blade turbines is approximately 51%, whereas it is reported to be 49% for two-blade turbines. In this paper, we examine the literature to determine the effect of the number of blades on the efficiency of wind turbines and the power generated.

The number of blades is very important because it affects the speed and efficiency of a turbine.The power that a wind turbine extracts from the wind is directly proportional to the swept area of the blades; consequently, the blades have a direct effect on power generation. The more blades that a wind turbine has, the more torque it produces (force that produces rotation) , and the slower the rotation speed (due to the increased drag caused by resistance to wind flow). Typically, turbines that are used to generate electricity must run at high speeds and, hence, do not require much torque. Thus, greater power generation results from a fewer smaller number of blades. In general, most horizontal axis wind turbines have three blades.

The decision to design three-blade turbines was a compromise. Due its reduced drag, a one- blade design is the optimal number for maximum efficiency. However, a single blade causes imbalance and, hence, is not practical.

A number of blades greater than three produces greater wind resistance, lower power generation and, therefore, is less efficient than three-blade turbines. For example, two-blade wind turbines face an unbalanced torsional force acting at the center (and supporting pole) of the blade. This unwanted twist can reflect to the blades, causing them to vibrate. If the rotating speed is equal to the natural vibration frequency of the blades, catastrophic mechanical damage can result. With three or more blades, the mechanical behavior of the turbine is practically the same for every possible blade orientation. The maximum number of blades that will produce maximum power on a particular size turbine is four.

Mechanical problems with two-blade turbines can be solved in a four-blade design, but ignoring the extra weight of the blade, economically four blades are more expensive than three blades. For thesereasons, turbines manufactured with three blades represent an ideal compromise between highenergy output, high stability, light weight, and turbine durability. A fewer number of blades increases flow speed, while a larger number of blades results in higher torque. The highest power is between these two extremes. Figure 3 compares the coefficient of electricity with the speed of the tip of a wind two and three blades.

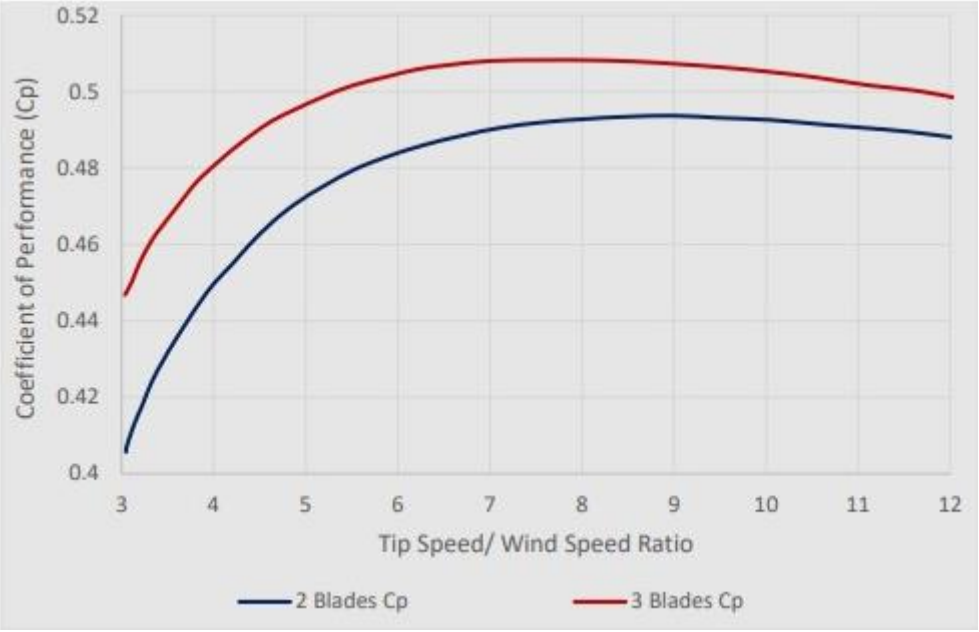


*Figure 3 The power coefficient versus tip speed of a two bladed and three bladed wind turbine*

## 2.1.1) Comparison of two and three bladed Wind Turbines

**1.) Performance and efficiency :**

Two-blade wind turbines are slightly less efficient than three-blade wind turbines and must rotate faster for maximum efficiency. Similarly, two blades will produce more electricity than three blades, but have their own problems. Two-blade turbines are sensitive to gyroscopic precision, which results in wobbling. Naturally, this wobbling will cause stability problems for the entire turbine. This will also put pressure on the turbine's components, reducing its efficiency and lifetime. According to the latest research, a two-blade design for a wind turbine is 3% less efficient than a three-blade counterpart of the same diameter. Additional power can be obtained from the longer wind turbine blades, with the advantage of lower construction, material and maintenance costs. Five-blade wind turbines greatly improve annual performance in poor wind conditions in areas.

**2.) Balance:**

A rotor with an even number of blades can cause stability problems in a rigid frame machine.The reason is that the moment from the upper blade is reflected back, and it achieves its maximum wind power and the lower blade passes through the wind shade in front of the tower. Wind turbine's three-blade rotor has more consistent performance than two or four blades.

**3.) Cost:**

The economic benefit of two-blade wind turbines is associated with lower manufacturing andtransportation costs. Research from a previous feasibility study reported that two-blade turbines cost 10−12% less than three-bladed units for offshore wind farms under certain operating conditions,

**4.) Weight:**

Two blade wind turbine designs have reduced cost and weight as compared to a three-blade rotor. Two-blade wind turbines are 30% lighter than three-blade wind turbines. Lower weightis a particular advantage for offshore application, as are ease of handling, transportation and assembly.

**5.) Rotor vibration :**

Two-blade wind turbines withstand an unbalanced twisting force acting on the hub (and pole) at twice the speed of the blade. This unwanted deflection can return to the blade, causing themto vibrate. A three-blade turbine on the other hand, has very little vibration. The reason for thisis that when one blade is horizontal, its two resistances are balanced by the other two blades. So, a three-blade turbine is the best combination of high rotational speed and minimum stress.The hub mechanism and/or post itself may need to be made stronger or more rigid to resist these unwanted torsion forces. In addition, it is expected that load reduction techniques to reduce the effect of load imbalance on the two-blade rotor, such as teetered hub, reduce the high natural vibration of the two-blade rotor by reducing the energy performance of the asymmetric configuration will make it better.

**6.) Noise:**

Two blade wind turbines must rotate faster for maximum efficiency. This is a disadvantage foronshore wind turbines, because the noise increases due the increase in tip speed, whereas increases in the number of blades lowers blade speed, which reduces the sound of wind turbines.

**7.) Wake effect:**

The turbulent intensity, however, indicates a high variability for the two-blade rotors. The intensity of the turbulence is particularly high in the tip area, due to the strong vortices generated. This higher level of turbulence in the wake supports higher wake recovery rates intwo-blade rotors than three bladed rotors, especially behind the turbine.

**8.) Aesthetics:**

Another factor influencing the number of blades is aesthetics. It is generally accepted that a three-blade turbine is more satisfying to the eye than one- or two blade-turbines. Although, itworth noting that five-blade wind turbines are more visually appealing than three-blade turbines.

**9.) Storm resilience:**

The main disadvantage of areas with frequent strong winds is that they can turn into regularviolent storms and hurricanes. Most wind turbines cannot withstand high wind speeds in

stormy conditions. Two-blade wind turbines can be easily erected into position and then laidback down on the ground with one crane instead of two if necessary in preparation for a storm. However, five-blade wind turbines greatly reduce the chance of malfunction, which ensures operational reliability in the long run.

## 2.3) Average Wind Speeds by regions in Turkey

Wind energy is an energy source that is valid all over the world, and its use is possible with a structure that converts the kinetic energy of wind speed into mechanical energy, with the principle of turning a turbine, and converts it into electrical energy through a generator. The unstable and variable nature of wind creates pauses and difficulties in its use on power systems. In the years just before 2000, wind analyzes began to receive more attention on issues such as a potential energy source and emission reduction strategies, as a requirement of environmental and public policies.

According to data from 2017, it is estimated that the rate of electricity production with wind energy in renewable energy sources is around 17%. But its total capacity is 23%. At the end of about thirty years, the usage rate is expected to approach 40% and provide more than 4 Terawatts of power, while fossil fuels are still used as the primary source with over 80% usage. Turkey's total wind energy electricity production rate reached 9.22% in the first two quarters of 2021 and continued its growth and development in the energy sector. The winds in the west of Turkey cover a significant part of the potential, and its total capacity grew by 15.19% in 2020 compared to the previous year.

When Turkey's one-year average wind model forecast map Figure 16 is examined in the section below, average wind speeds of 3-5 m/s per second are estimated throughout Turkey. On an annual average, the Mediterranean, Central Anatolia and Aegean regions have wind speeds of 4 m/s and above, which is suitable for power generation. It has been determined that the southern and western regions of Turkey have above average temperatures. Northern and central regions are predominantly closer to average, although in the eastern regions the model produced generally colder forecasts.

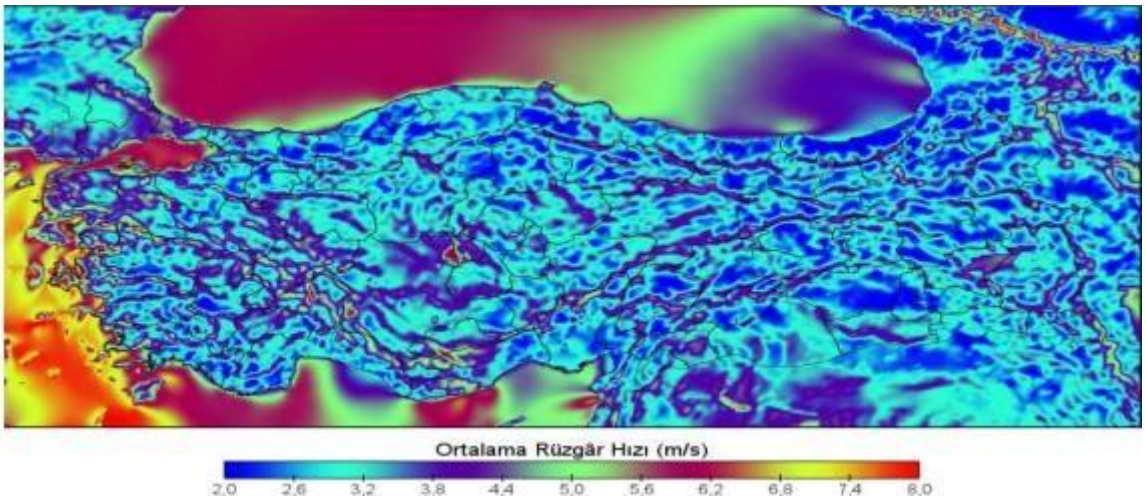


*Figure 4 Turkey Annual average Wind Speed Map*

In the scatter chart created with hourly wind speed measurement data of different provinces and regions of Turkey over a one-year period, Hatay generally has a more homogeneous appearance than other regions and is associated with higher speeds on average. However, in model predictions, Hatay displays a different image. . In measurements, Çanakkale shows a similar distribution to Hatay. While the average wind speeds in the Manisa region have the lowest speeds throughout the year, and when evaluated in terms of speed intensities, it is seen that the order is Çanakkale, Hatay, Balıkesir, İzmir Güzelyalı, İzmir Çeşme and Manisa, respectively.

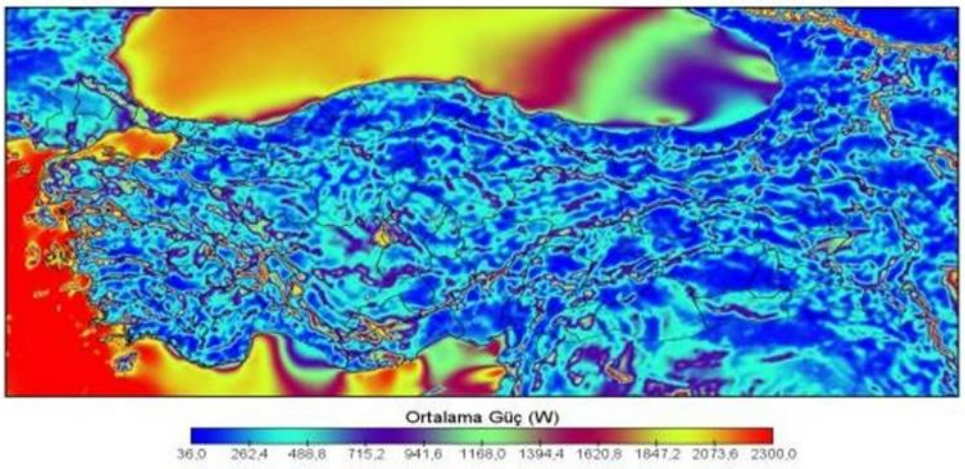


*Figure 5 Türkiye 2.3 MW wind power production potential map*

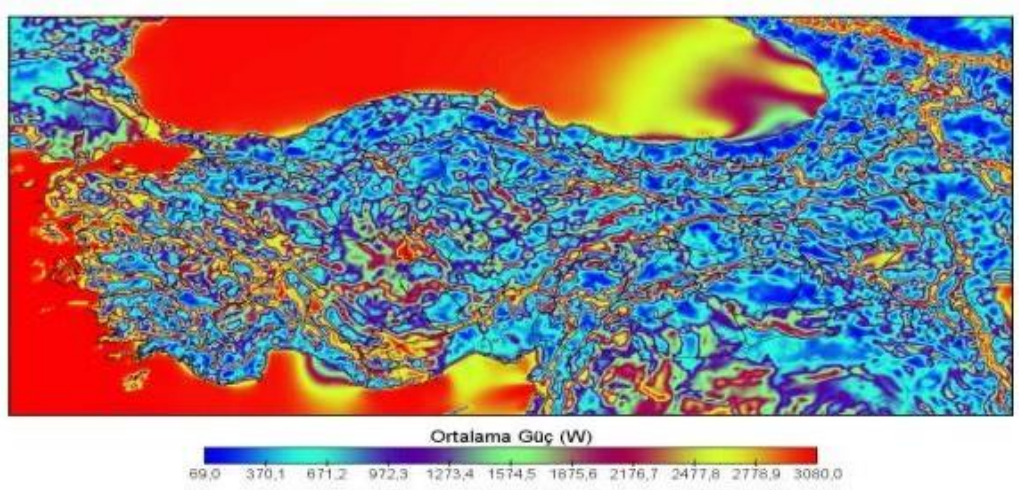


*Figure 6 Türkiye 3 MW wind power production potential map*

In Turkey, wind energy generation potential of 2.3 MW and 3 MW is estimated. Although there are 2.3 MW production areas, power generation maps indicate that 3 MW investments can yield much better results in the long term.

With all these parameters, the average wind speed in the Central Anatolia region of Turkey is around 5 m/s. This report will take this speed as a reference.

## 2.4) Blade Aerodynamics and Acting Forces

### 2.4.1) Airfoil Blade:

In order to obtain effective energy, modern wind turbines are produced in the form of airfoil sections. This form was used by NACA. For example, angles and concepts on a NACA profile are shown in section:

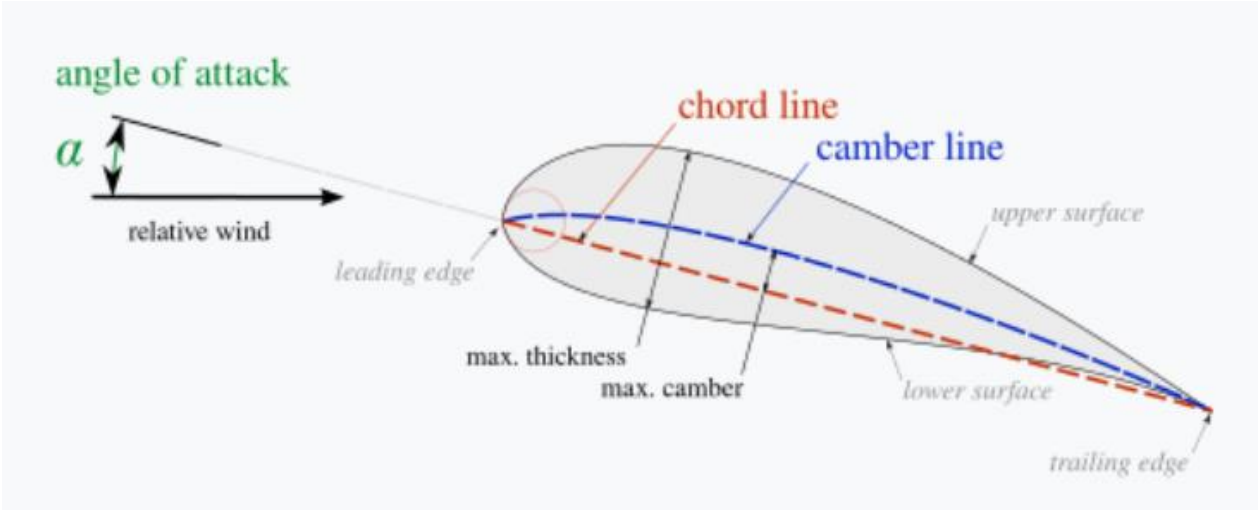


*Figure 7 Airfoil Section*

The geometry of the airfoil is described with a variety of terms :

**The leading edge** is the point at the front of the airfoil that has maximum curvature (minimum radius).

**The trailing edge** is the point on the airfoil most remote from the leading edge. The angle between the upper and lower surfaces at the trailing edge is the trailing edge angle.

**The chord line** is the straight line connecting leading and trailing edges. The chord length, or simply chord, c is the length of the chord line. That is the reference dimension of the airfoil section.

**Angle of Attack (AoA):** The angle between the chord line and the relative wind speed is called the angle of attack. When an airfoil section of a blade is exposed to the wind, air flows above and below the section, but the air flowing below is slower (V1 > V2).

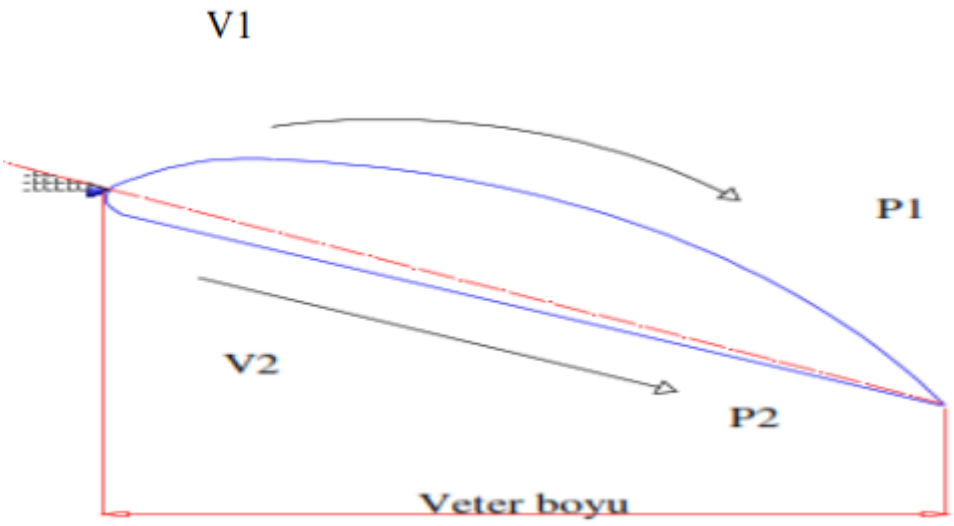


*Figure 8 Pressure and Velocity Acting on the Turbine Blade*

From Bernoulli Equation:

$$\frac{P_1}{\rho g} + \frac{V_1^2}{2g} + h_1 = \frac{P_2}{\rho g} + \frac{V_2^2}{2g} + h_2 \qquad (1)$$

$$P_2 > P_1$$

As a result of this situation, low pressure occurs in the upper part of the section, and F force occurs due to this pressure difference. This force F has two components: Lift force $F_L$ and Drag force $F_D$.

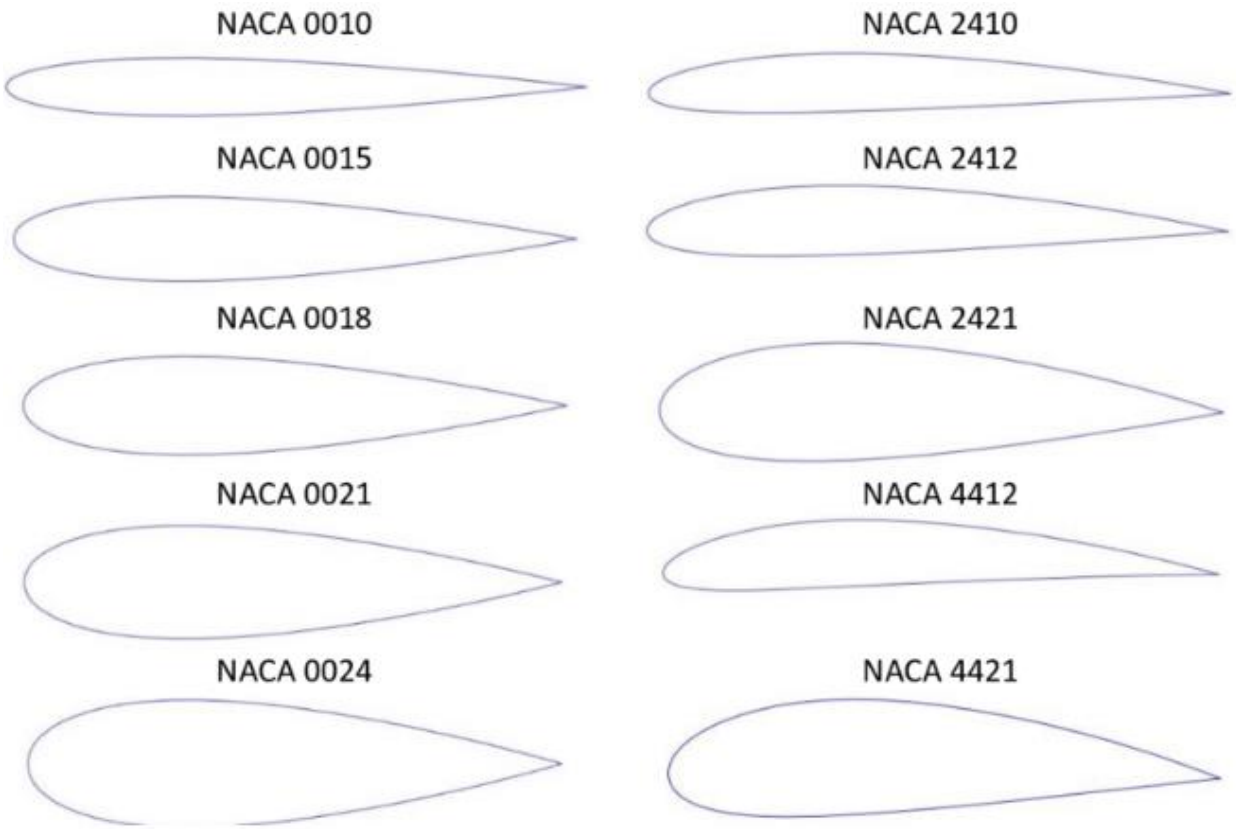


*Figure 9 NACA Airfoils*

## 2.4.2) NACA Profiles Comparison

NACA (National Advisory Committee for Aeronautics) airfoils are standard airfoil shapes used in aeronautical engineering for aircraft wings and other aerodynamic surfaces. These profiles were developed in the 1930s by the committee in the United States. NACA airfoils are designed to optimize aerodynamic characteristics and have been widely used in aviation applications.

In this section, the $C_L$ and $C_D$ values of different NACA airfoils were examined and the results were compared.

When the results of the analyzes performed at different angles of attack were examined, the calculated $C_D$values for each airfoil model were given in Figure 10. The $C_D$ value of the Curtis C-72 model was found to be the highest at all angles of attack values except 0°. On the other hand, the $C_D$ value of NACA 4418 was the highest at 0°, then decreased and was calculated to be the lowest at approximately 10° and higher angle of attack values. The $C_D$ values of the other airfoil profiles were observed to be close to each other at all angles of attack values. In general, it was observed that the Cd value increased with increasing the angle of attack in all airfoils. The $C_D$ value varied between 0.0303 and 0.5932.

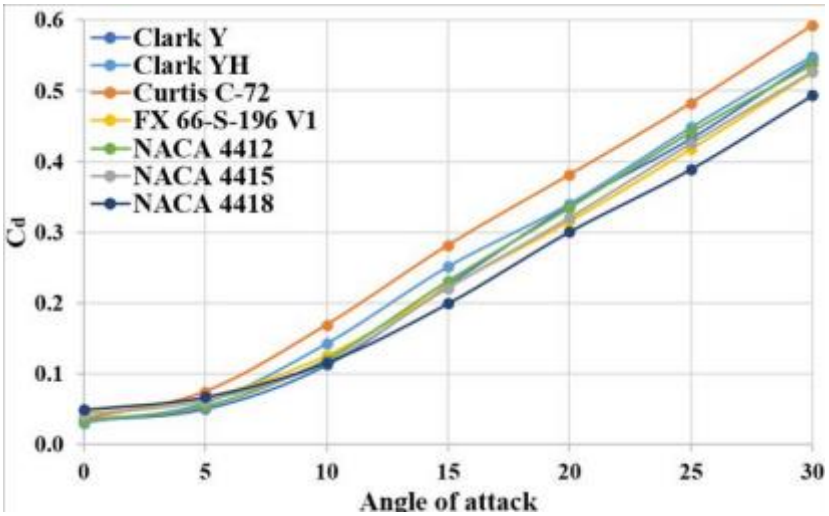


*Figure 10 The calculated Cd values for all airfoil profiles*

The distribution of $C_L$value was given in Figure 11. While the angle of attack value increased the lifting force up to a certain point, it caused a decrease in this value after a point. The $C_L$ value, which increased up to about 10°, decreased a little after this point and then remained horizontal. When similar studies in the available literature were examined, it was seen that the highest $C_L$ values were calculated at between 10 and 15° angle of attack conditions. While Curtis C-72 had the highest lift force up to about 10°, then the highest value was seen in NACA 4415. The lowest $C_L$ value at all angles of attack conditions was seen in the Clark YH model. After about 15°, it was observed that the $C_L$ value was around 1 in other models except for FX 66-S-196 V1 and Clark YH models. The $C_L$ value varied between 0.2507 and 1.1699, and they showed these values at 0 and 10° angle of attack conditions, respectively.

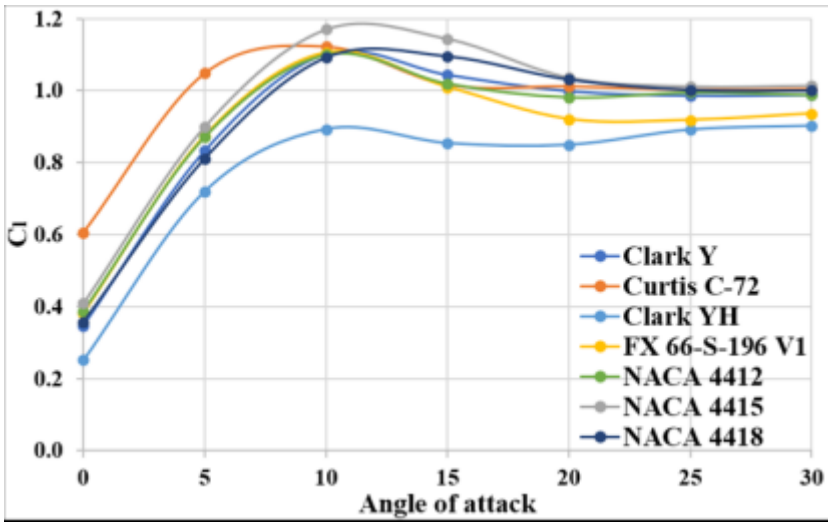


*Figure 11 The calculated Cl values for all airfoil profiles*

Comparisons of the results obtained from the GRA analyzes performed separately for each angle of attack were presented in Figure 12. According to these results, the best case is Curtis C-72 at 0 and 10°, and Clark Y at 5°. The worst cases at 0, 5, and 10° were observed in NACA 4418, FX 66-S-196 V1, and Clark Y, respectively. At angles of attack values above 10°, the best case was seen in NACA 4418, which had the lowest Cd coefficient in general. In the same conditions, the worst case was seen in the Clark YH model, which had the lowest Cl coefficient at all angles of attack conditions.

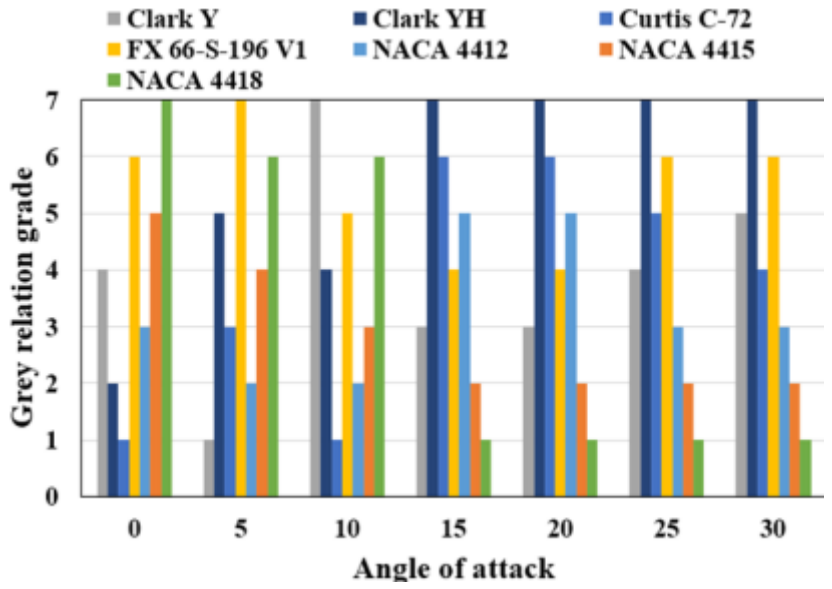


*Figure 12 The comparison of Grey relation values for all airfoil profiles*

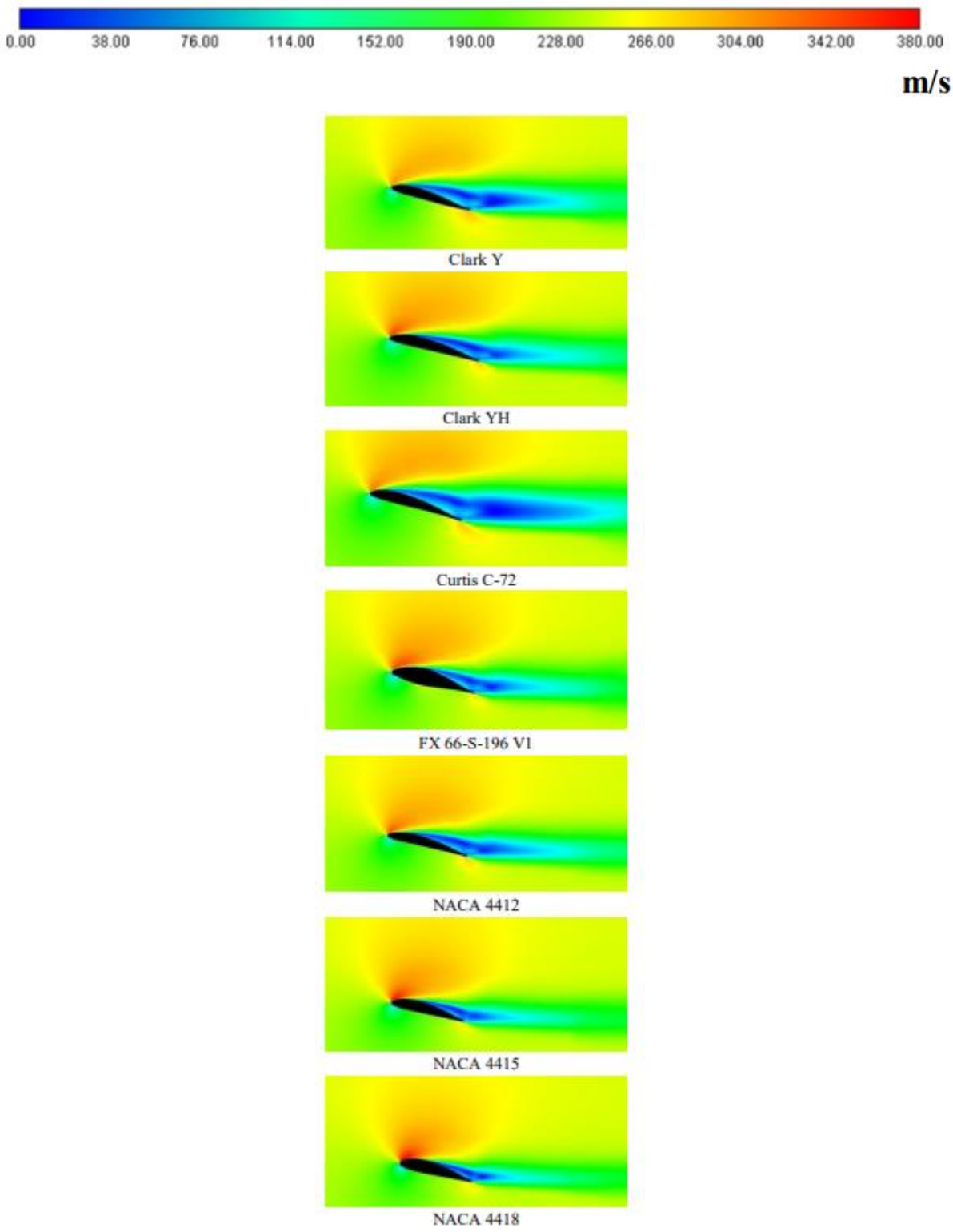


*Figure 13 . The velocity distribution of all airfoil profiles at 15°*

Based on these results and analyses, we decided to make the comparison using the **NACA 4415** airfoil in our own wind turbine blade design.

## 2.5) Betz Limit, Power and Torque in Wind Turbines

Wind energy depends on the area of the propeller, the cube of the wind speed and the density of the air.

The energy to be obtained depends on the efficiency of the turbine.

The power carried by the wind:

$$P = \frac{1}{2}\dot{m}V_r{}^2 \tag{2}$$

Mass Flow Rate:

$$\dot{m} = \rho * A * V_r \tag{3}$$

If we apply the mass flow equation to the power formula,

$$P = \frac{1}{2} * \rho * A * V_r^3 \tag{4}$$

Where, $P$ is the power (in watts), $A$ = area swept by the propeller ($A = \pi r^2$) , $r$ rotor radius) and $V_r$ is the wind speed (in $m/s$).

Density of air at sea level $\rho = 1.225\ kg/m^3$.

While the theoretical calculation of a wind turbine's power is possible, determining the actual power output from the wind in practice is not straightforward. As the wind flows over the turbine, only a portion of its kinetic energy is transferred to the system. This energy transfer occurs according to a specific coefficient, known as $C_P$, which is referred to as the Betz limit.

$$C_P = \frac{1}{2} * \frac{P_r}{\rho * A * V_1^3} \tag{5}$$

$P_r = Power\ generated\ by\ turbine$

$\rho = Density\ of\ Air$

$A = Area\ swept\ by\ the\ turbine$

$V_1 = Wind\ Velocity$

Here we find $P_r$ as follows:

$$P_r = \frac{1}{2} pAV_1^3 C_p \tag{6}$$

Theoretically, we achieve efficiency when we compare the data we obtain at the maximum point with the power value actually obtained.

## 2.6) Mechanical Power from Wind

The kinetic energy of the air fluid with mass $m$ and speed $V_r$ is;

$$E = \frac{1}{2} mV^2 \tag{7}$$

The derivative of energy with respect to time gives power;

$$\frac{dE}{dt} = \frac{1}{2} \dot{m}(V_1^2 - V_3^2) \tag{8}$$

$$P_r = \frac{1}{2} \dot{m}(V_1^2 - V_3^2) \tag{9}$$

$\dot{m} = \text{Mass Flow Rate}$

$$\dot{m} = \rho A \frac{1}{2}(V_1 + V_3) \tag{10}$$

$$P_r = \frac{1}{2}\left(\rho A \frac{1}{2}(V_1 + V_3)\right) * (V_1^2 - V_3^2) \tag{11}$$

$$P_r = \frac{1}{2}\rho A V_1^3 * \left(\frac{1}{2}\left(\frac{V_1}{V_1} + \frac{V_3}{V_1}\right) * \left(\frac{V_1^2}{V_1^2} - \frac{V_3^2}{V_1^2}\right)\right) \tag{12}$$

$$P_r = \frac{1}{2}\rho A V_1^3 * C_P \tag{13}$$

The magnitude of wind power depends on Cp. If we write $\lambda = \frac{V_3}{V_1}$,

$$C_P = \frac{1}{2}\left(\frac{V_1}{V_1} + \frac{V_3}{V_1}\right) * \left(\frac{V_1^2}{V_1^2} - \frac{V_3^2}{V_1^2}\right) \tag{14}$$

$$C_P = \frac{1}{2}(1 + \lambda) * (1 - \lambda^2) \tag{15}$$

Here, $C_P$ is efficiency of rotor. If we want to find maximum rotor efficiency Cp to λ If the derivative is taken according to and equalized to zero;

$$0 = 1 - 2\lambda - 3\lambda^2 \tag{16}$$

We obtain this expression.

$For\ \lambda = -1\ and\ \lambda = 1/3\ , C\_P = 0.5926\ reaches\ maximum\ value.$

This means that we can obtain at most 59.26% energy from wind.

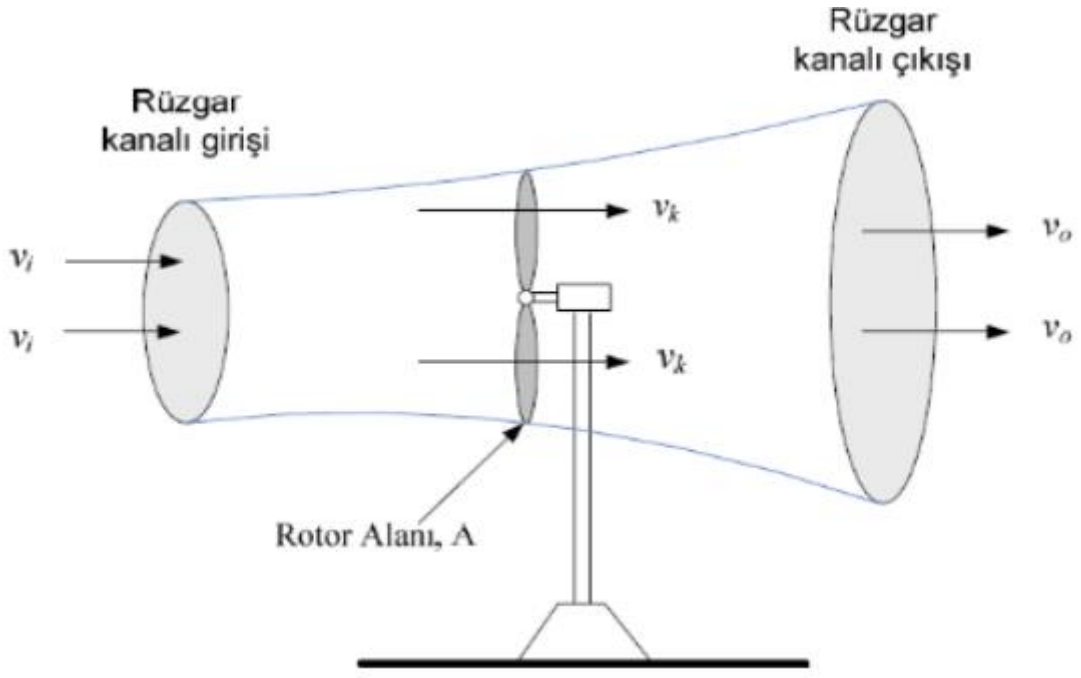


*Figure 14 Wind velocities acting on the blade*

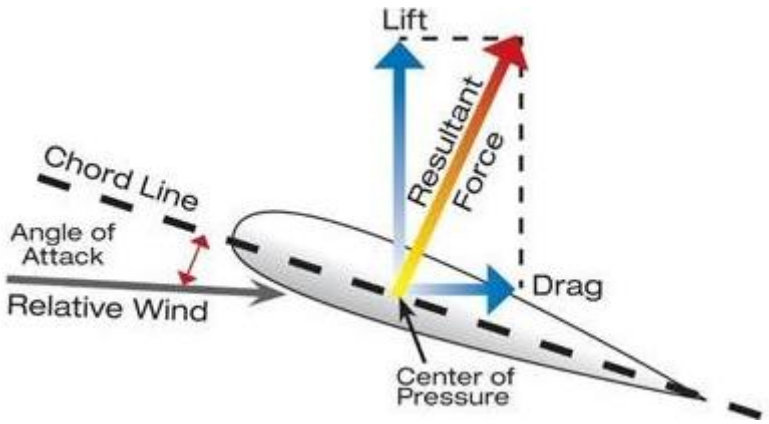


*Figure 15 Lift and Drag Forces on Airfoil*

The lift and drag coefficients of a real blade can be determined through wind tunnel experiments or computed using CFD (Computational Fluid Dynamics). These coefficients, $C_L$ and , $C_L$, are influenced by the shape of the airfoil. The figure above illustrates how , $C_L$ and , $C_D$ change depending on the angle of attack $\alpha$.

The lift and drag coefficients are evaluated in wind tunnels under varying wind velocities and angles of attack. For each angle, the ratio of $C_L$ to $C_D$ is calculated. The angle of attack that yields the highest $C_L/C_D$ ratio is considered the most efficient for maximizing the performance of wind turbines.

**Lift Coefficient:**

$$C_L = \frac{L}{0.5 * \rho * V_1^2 * c} \tag{17}$$

**Drag Coefficient:**

$$C_D = \frac{D}{0.5 * \rho * V_1^2 * c} \tag{18}$$

$F_L$ and $F_D$ can be obtained by taking the Lift and Drag Forces from these formulas.

# 3.) DESIGN AND PROCESS

## 3.1) Airfoil Optimization

In this project, a control volume was created for airfoil optimization. In present analysis, C type mesh with three-way velocity inlet method is used. The close view of geometry, mesh and boundary condition used in analysis is shown in Fig 16 and Fig.17. The $\frac{C_L}{C_D}$ values of the airfoils in the first five panels were maximized. Twist angle was determined where $\frac{C_L}{C_D}$ is maximum.

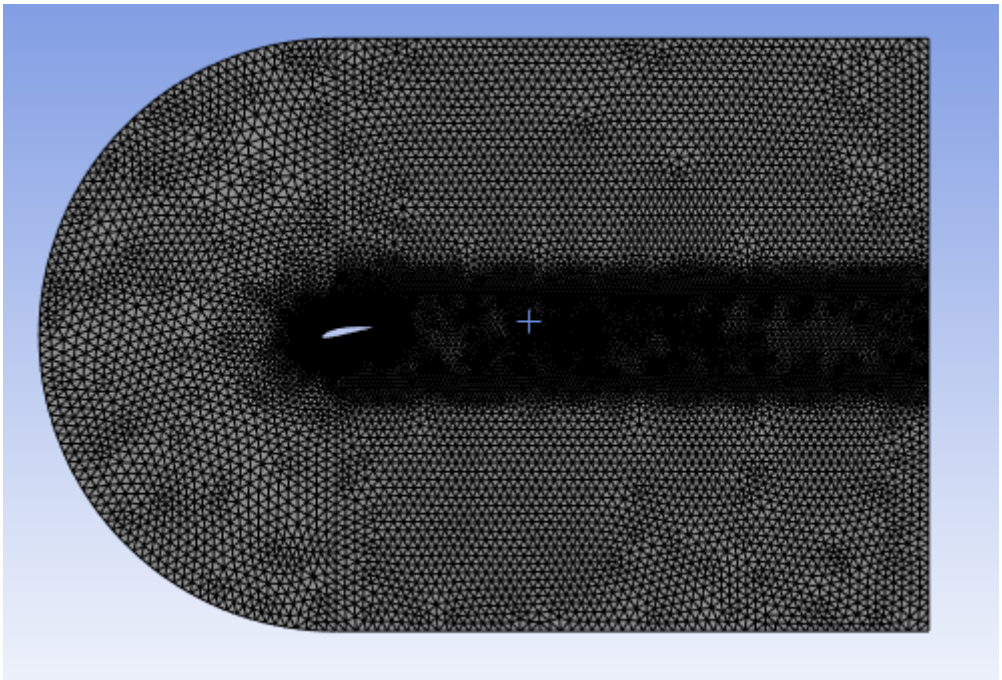

*Figure 16 Mesh Generation of NACA 4415*

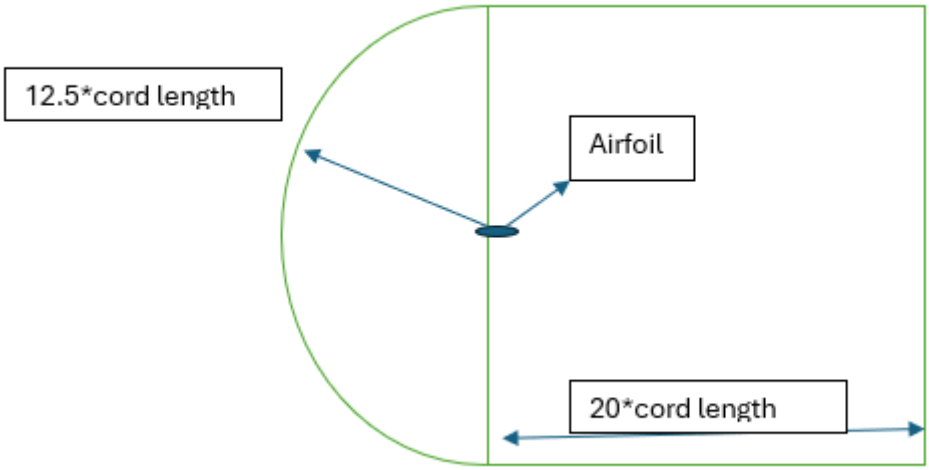


*Figure 17 C-type mesh construction*

*Tablo 1 Angle of Twist table*

| Chord Number | Angle of Twist | CL/CD |
|---|---|---|
| 1 | 10 | 43.589 |
| 2 | 8.1569 | 44.469 |
| 3 | 7.5037 | 43.482 |
| 4 | 7.292 | 41.944 |
| 5 | 5.5662 | 44.408 |

## 3.2) Modeling the Blade

In this project, NACA 4415 airfoil structure was used to model the blade. x, y and z coordinates were taken for modeling via Airfoil tools. When creating the blade structure, a plane should be assigned for each interval where the blade form changes, and blades with different chord lengths and twist angles should be created on these planes profiles should be created.

*Table 2 NACA 4415 Blade Design Features*

| Plane | Span | Chord Length | Twist Angle |
|---|---|---|---|
| 1 | 0 | 800 | - |
| 2 | 900 | 1464.1 | 10 |
| 3 | 1200 | 1331 | 8.1569 |
| 4 | 1500 | 1210 | 7.5037 |
| 5 | 1800 | 1100 | 7.292 |
| 6 | 2100 | 1000 | 5.57 |
| 7 | 2400 | 900 | - |
| 8 | 2700 | 810 | - |
| 9 | 3000 | 729 | - |
| 10 | 3300 | 656.1 | - |
| 11 | 3600 | 590.49 | - |
| 12 | 3900 | 531.441 | - |
| 13 | 4200 | 478.297 | - |
| 14 | 4500 | 430.467 | - |
| 15 | 4800 | 387.42 | - |
| 16 | 5100 | 348.678 | - |
| 17 | 5400 | 313.811 | - |
| 18 | 5700 | 282.43 | - |
| 19 | 6000 | 254.187 | - |
| 20 | 6300 | 228.768 | - |
| 21 | 6600 | 205.891 | - |

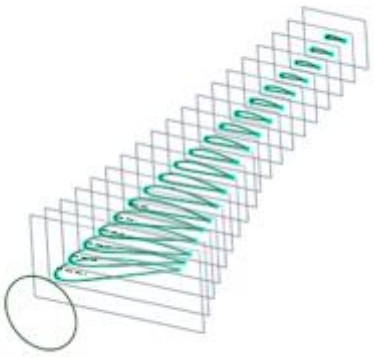

*Figure 18 Wind Turbine Blade Planes*

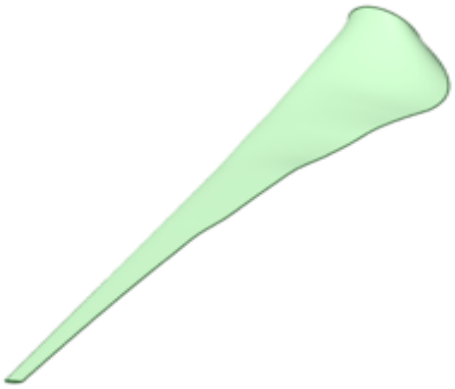

*Figure 19 Turbine Blade*

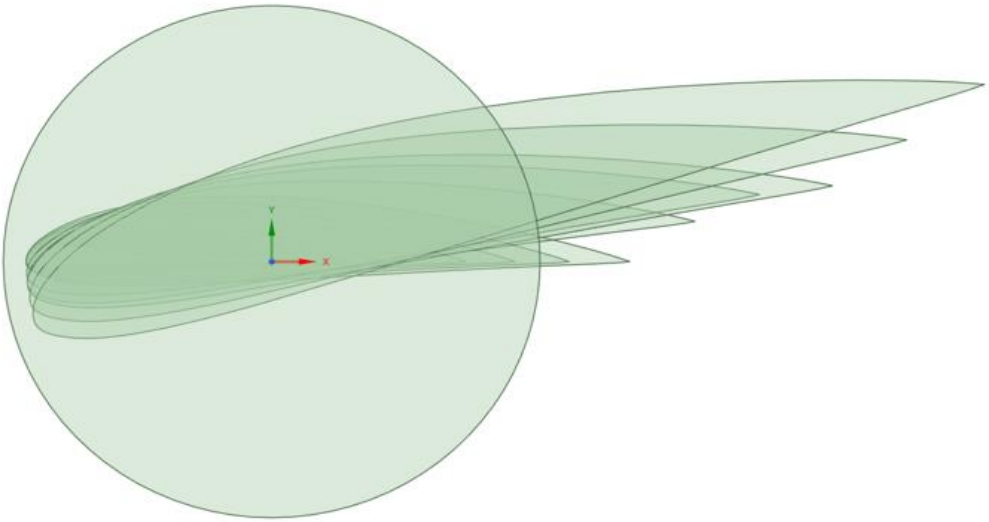

*Figure 20 All completed Blade Profiles*

## 3.3) Winglet Optimization

The dimensions of the bioinspired winglet were calculated based on the scaling factor, winglet length, and winglet sweep angle. The chord lengths used in the winglet and the tip height of the winglet were determined through optimization. Subsequently, the control volume (Flow Domain) for the winglet was created.

In ANSYS FLUENT, the Lift Force on the winglet, Cl/Cd ratio, and induced drag were calculated. Additionally, a static analysis of the winglet was performed to determine the factor of safety, and the winglet was designed accordingly.

For Winglet, we obtained the values according to the ratio between the Reference values and our own values.

$$Span = 6600\ mm$$

$$Chord = 205.891\ mm$$

**Scale Factor for Span** ;

$$SF1 = \frac{6600\ mm}{89600\ mm} = 0.0736 \qquad (19)$$

**Scale Factor for Chord;**

$$SF2 = \frac{205.891\ mm}{1750\ mm} = 0.117652 \tag{20}$$

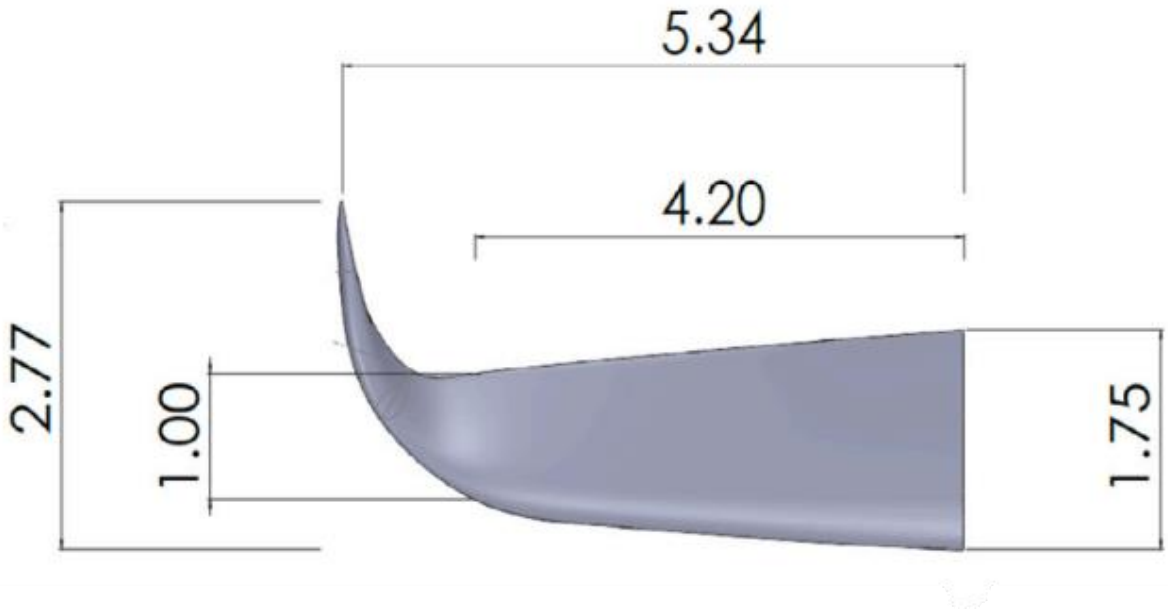


*Figure 21 Reference Winglet Dimensions*

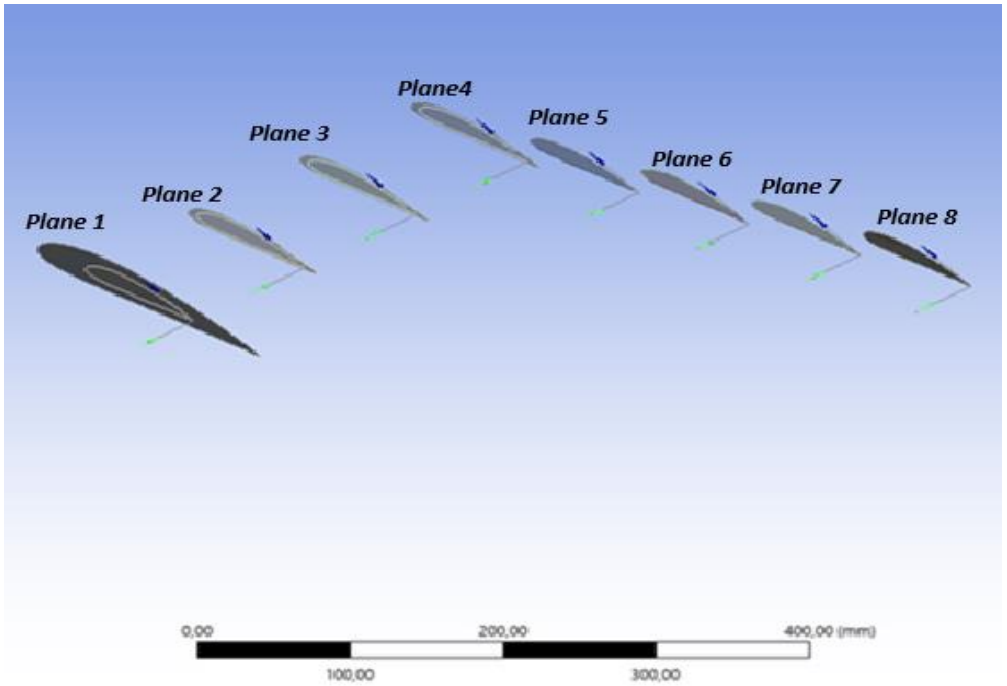


*Figure 22 Winglet Planes*

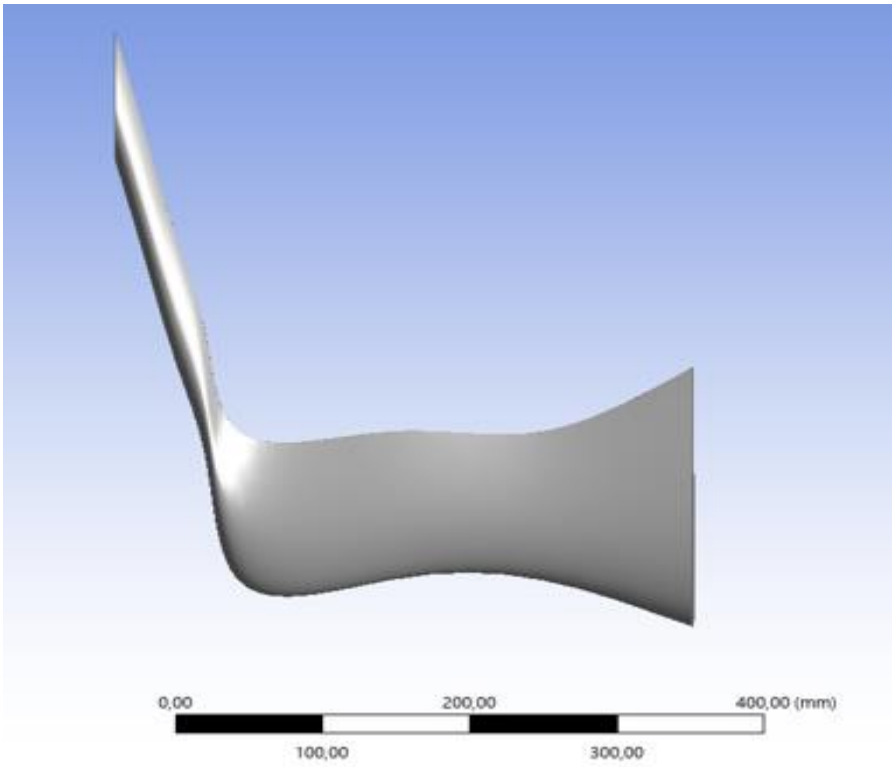


*Figure 23 Not Optimized Winglet*

### 3.3.1) Winglet Fluent Analysis

Winglet's span was determined as 393.024 mm. When creating the Flow Domain, the radius was determined as 5 times the winglet and the outlet distance was determined as 10 times the winglet.

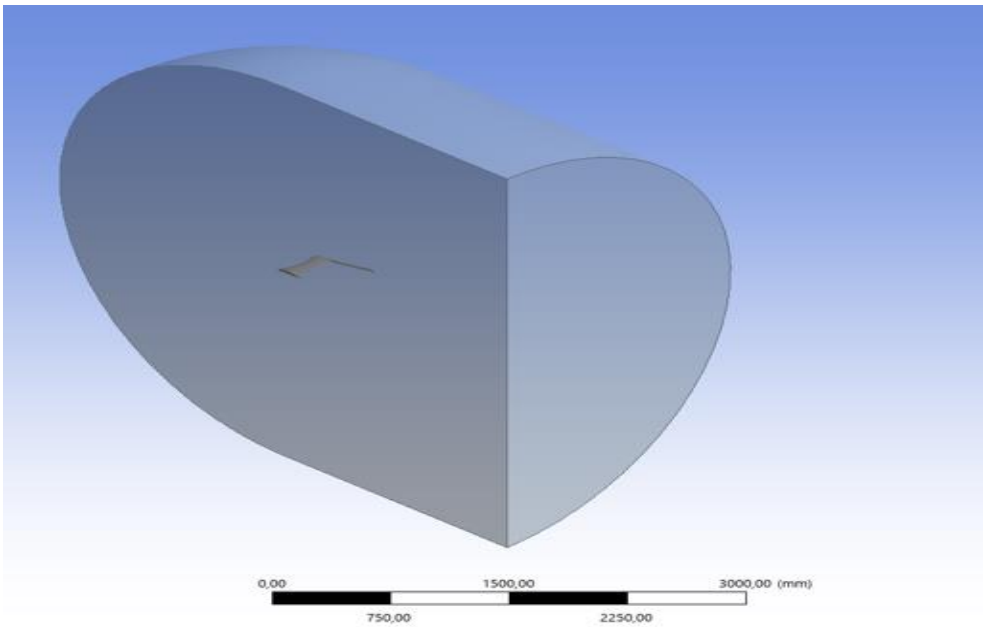


*Figure 24 Flow Domain of Winglet*

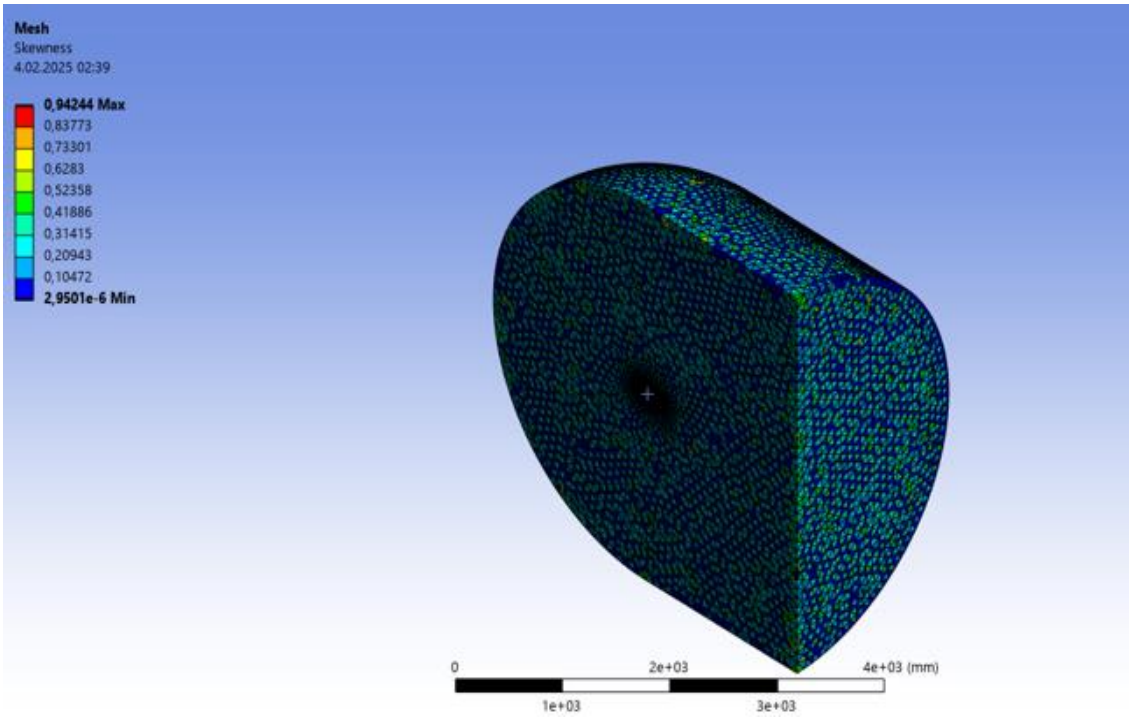


*Figure 25 Winglet Meshing Process*

k-w sst turbulence model was chosen and second order upwind method was chosen in the SIMPLE algorithm and indicated drag was minimized. Optimization was made to maximize lift force.

$$Di = \frac{L^2}{\pi e A \rho v^2}$$

$$A = Span/Cord$$

$$e = \ Oswald\ factor$$

$$e = 1.\ (Ideal\ Condition)$$

### 3.3.2) Winglet Static Structure

In the first Winglet design, Al 7075-T6 was utilized, and the static structural analysis yielded a FOS value of 15. Because of the excessive safety coefficient this value offers, weight

optimization has become necessary. Optimization was done using new material choices and geometry modifications because the ideal FOS value was found to be 2-3. Composite materials such as glass fiber reinforced polymer (CFRP) have been evaluated and the strength/weight ratio has been taken into account.

$$Factor\ of\ Safety = \frac{\sigma}{\sigma_{max}} \tag{21}$$

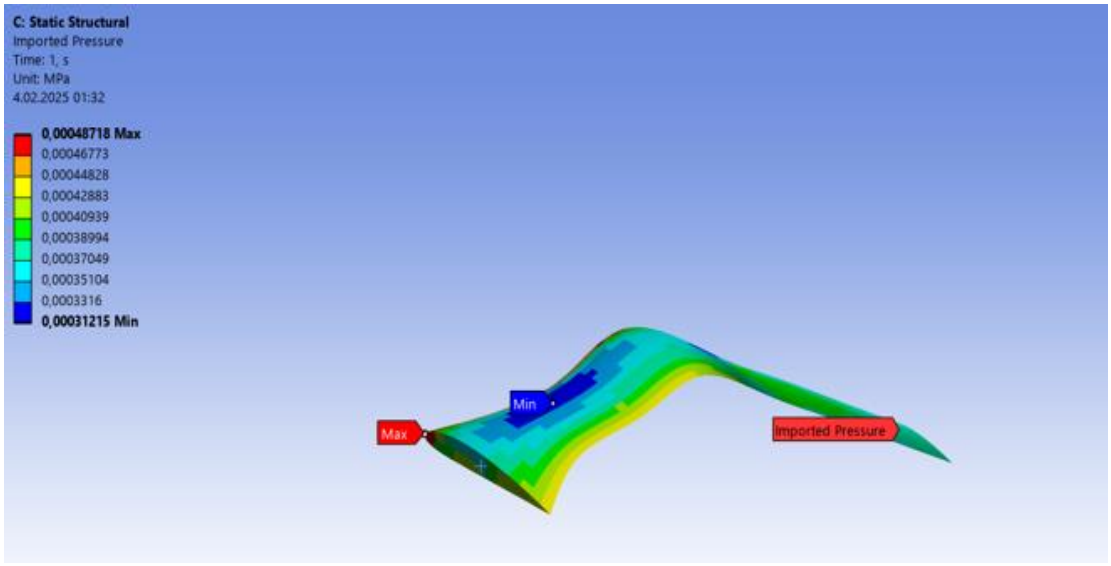


*Figure 26 Winglet Static Structural*

| Table of Schematic D2: Optimization | | | | |
|---|---|---|---|---|
| | A | B | C | D |
| 1 | Input Parameters | | | |
| 2 | Name | Lower Bound | Upper Bound | |
| 3 | P33 - Plane2_scale | 1,1765 | 2,0589 | |
| 4 | P34 - Plane3_scale | 1,1765 | 2,0589 | |
| 5 | P36 - Plane5_scale | 0,58826 | 1,1765 | |
| 6 | P37 - Plane6_scale | 0,29413 | 0,58826 | |
| 7 | P38 - Plane7_scale | 0,14707 | 0,29413 | |
| 8 | P39 - Plane8_scale | 0,073533 | 0,14707 | |
| 9 | P48 - Plane5_height (mm) | 0 | 30 | |
| 10 | P49 - Plane6_height (mm) | 30 | 60 | |
| 11 | P50 - Plane7_height (mm) | 60 | 90 | |
| 12 | P51 - Plane8_height (mm) | 90 | 120 | |
| 13 | P68 - Oswald factor | 0,7 | 1 | |

*Figure 27 Parameter Range*

The values obtained depending on these parameters are shown in the table.

*Tablo 3 Winglet Dimensions and Force*

| | Chord Length | Height |
|---|---|---|
| 1 | 205.89 mm | 0 |
| 2 | 184.99 mm | 0 |
| 3 | 154.32 mm | 0 |
| 4 | 117.65 mm | 0 |
| 5 | 64.946 mm | 17.199 mm |
| 6 | 46.51 mm | 37.632 mm |
| 7 | 19.929 mm | 84.091 mm |
| 8 | 11.767 mm | 94.241 mm |
| Average Chord | 97.001 mm | 0 |
| Span | 393.024 mm | 0 |
| Indicated Drag | 0.010847 | 0 |

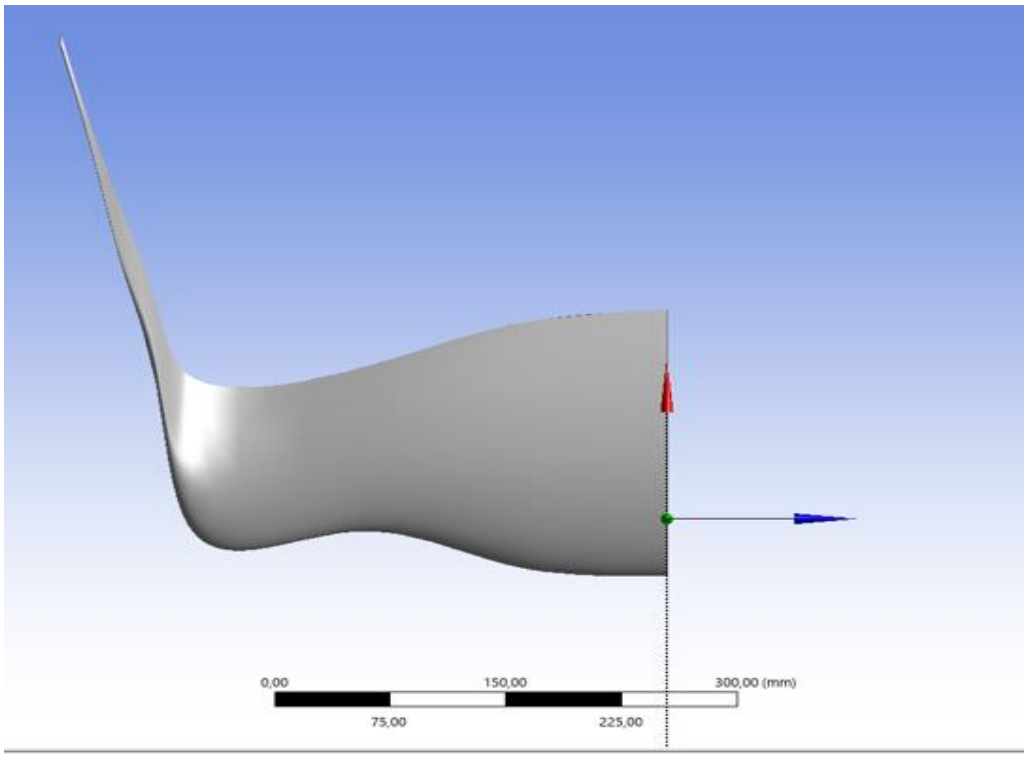


*Figure 28 Optimized Winglet*

## 3.4) Fluent Analysis of Wind Turbine Blade with Winglet

The created winglet was attached to the blade we created. As a result of the analysis and optimization, the most optimal Winglet + Blade length was obtained.

$$6600 + 393.024 = Winglet + Blade = 6993.024 \text{ mm}$$

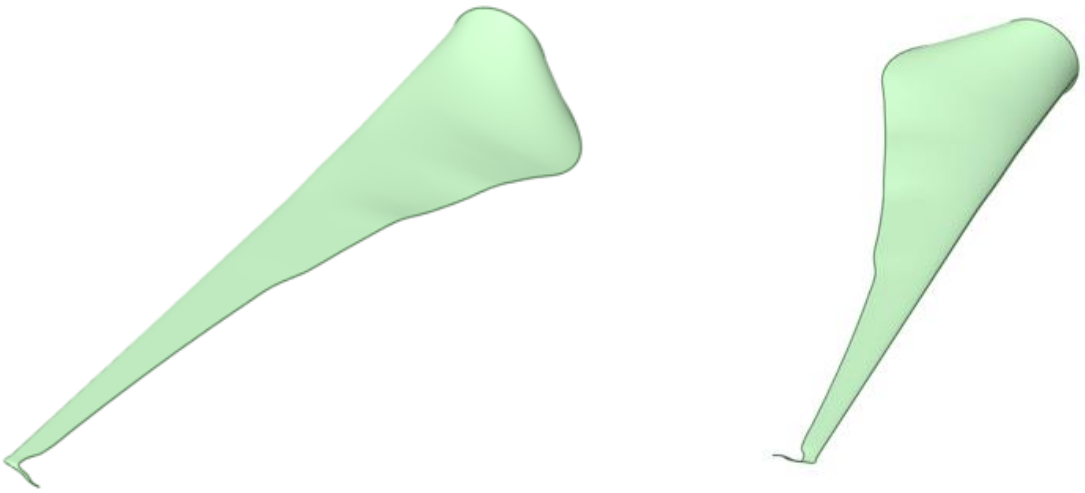

*Figure 29 Blade with Winglet*

Firstly, FLUENT is run in the Ansys workbench program. Then, a control volume is created to contain the blade.

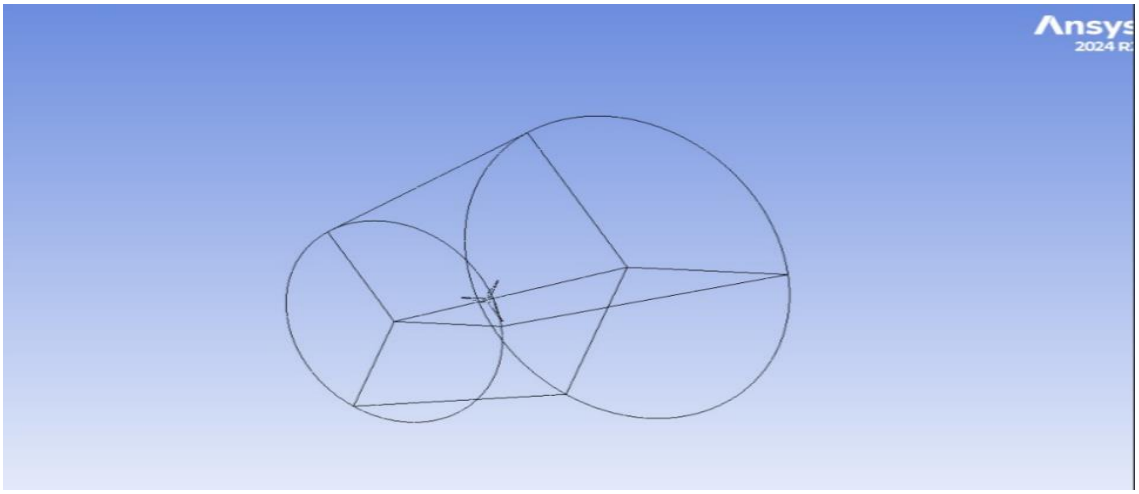

*Figure 30 Frame (Control Volume)*

Then, the meshing process of the control volume was started.

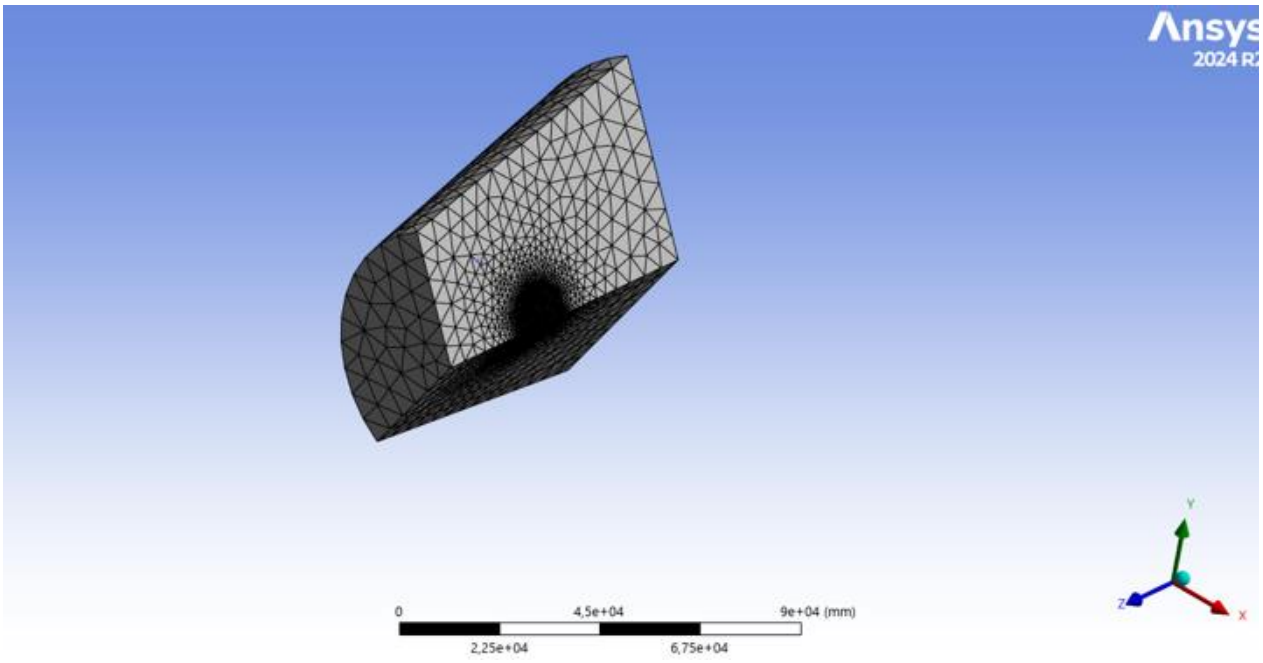


*Figure 31 Meshing the Control Volume 1*

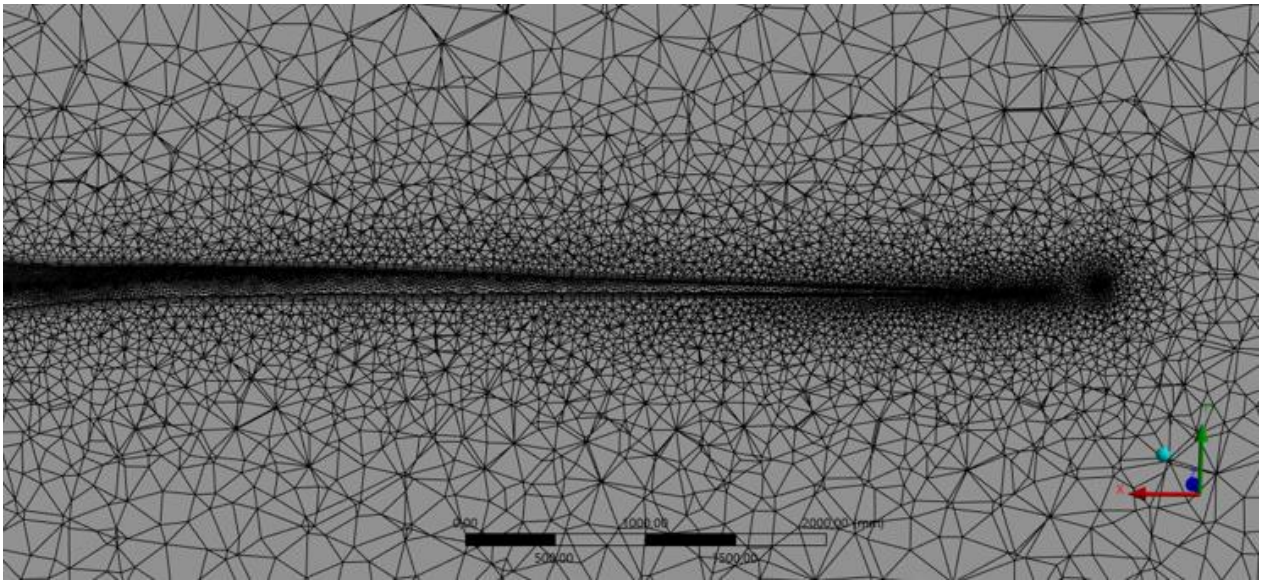

*Figure 32 Meshing the Control Volume 2*

In the next stage, the boundary conditions in the flow field were determined and the necessary calculations were made.

- Wind Velocity = 5 m/s
- Air pressure at the outlet
- Density of Air $\rho = 1.225\ kg/m^3$
- Viscosity of Air $\mu = 0.000017894 \frac{kg}{m} * s$
- Interfaces
- Flow Inlet
- Flow Outlet

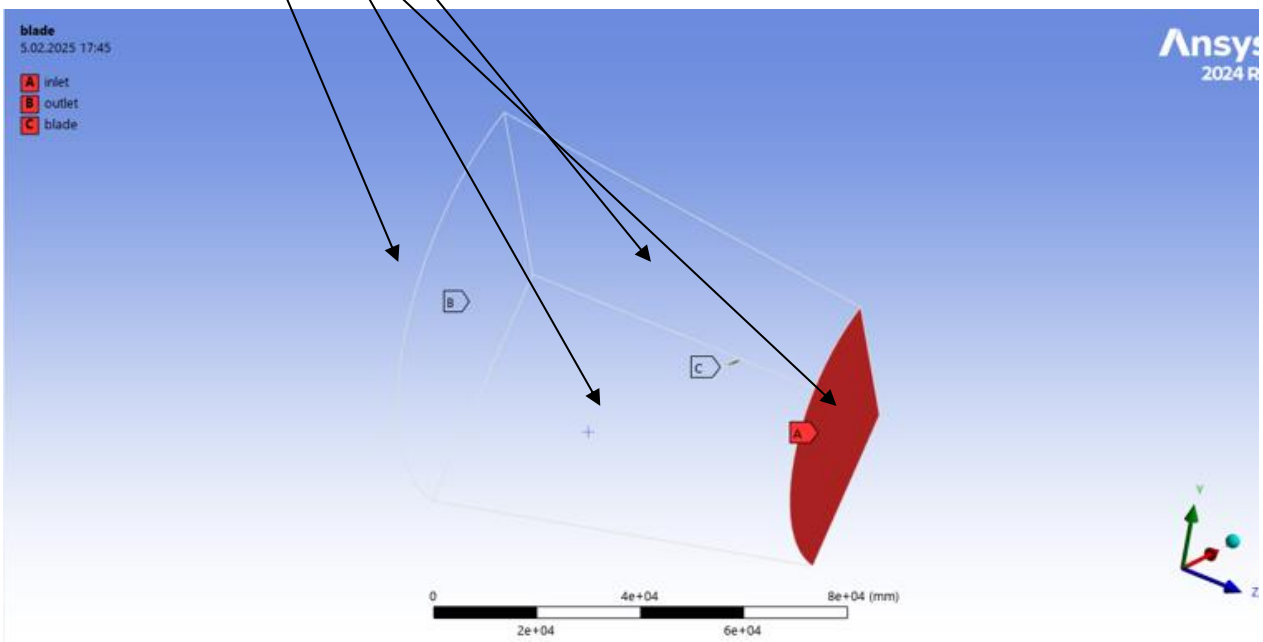


*Figure 33 Boundary Conditions*

In the Solution section, the solution will be performed according to the following settings:

- Properties of Air (Material Type)

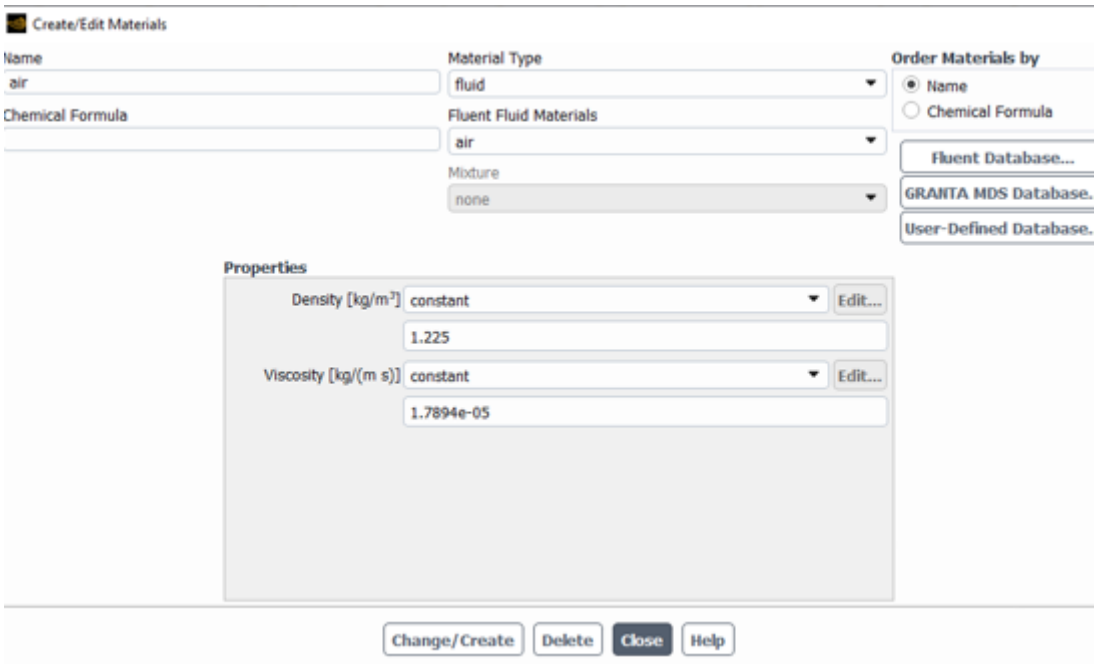


*Figure 34 Fluid properties in FLUENT*

To simplify the solution, the rotational velocity was taken as constant $\omega$ = 2.22 Rad/s.

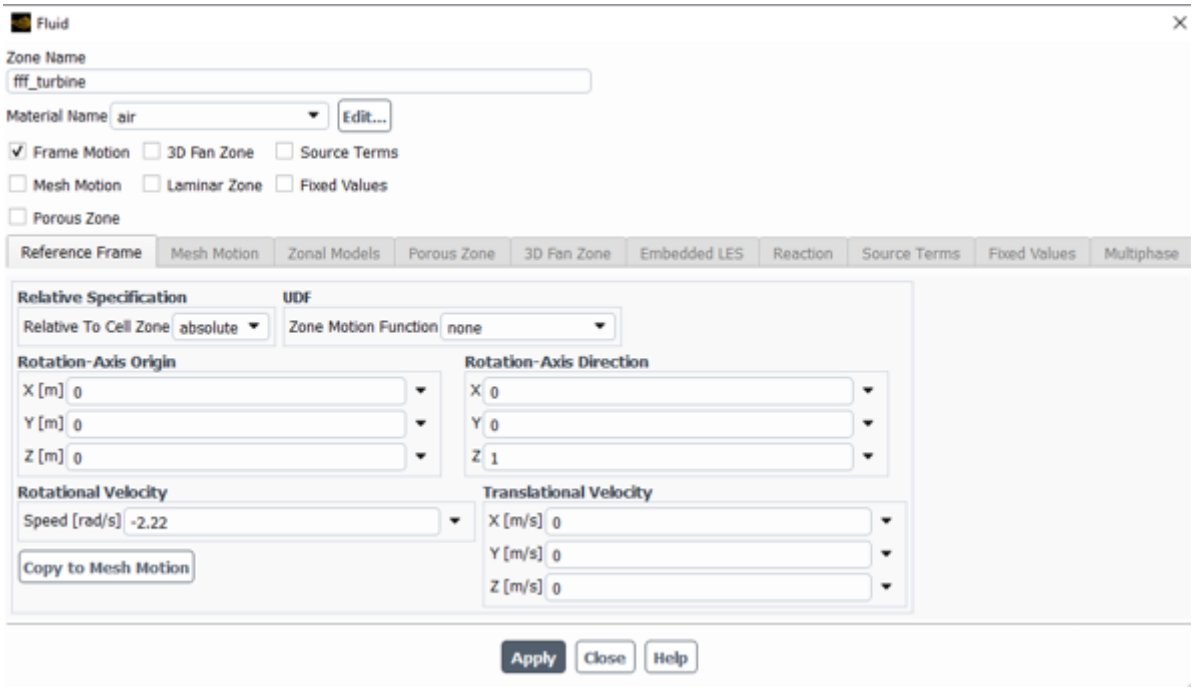


*Figure 35 Rotational Velocity Value*

Wind velocity and direction were entered in the (Boundary Condition) section. Our wind velocity 5 m/s. In the analysis study, **the number of iterations was taken as 150.**

## 3.4.1) Preliminary Analysis

The most important step to do before moving on to the results section is preliminary analysis.

### 1.) Equations Used

- In this analysis, the Continuity Equation "Law of Conservation of Mass" and the Navier-Stokes Equation "Law of Conservation of Momentum" are used.

- These equations are written in a rotating reference frame. It has the advantage of not requiring a moving mesh to calculate the rotation of the wing in its simulation.

- Contiunity Equation:

$$\frac{\partial \rho}{\partial t} = \nabla * \rho * \overrightarrow{\vartheta_r} = 0 \qquad (22)$$

- Navier-Stokes Equation:

$$\nabla * \left( \rho * \overrightarrow{\vartheta_r} * \overrightarrow{\vartheta_r} \right) + \rho\left(2 * \vec{\omega} \times \overrightarrow{\vartheta_r} + \vec{\omega} \times \vec{\omega} \times \vec{r}\right) = -\nabla p + \nabla * \bar{\tau_r} \qquad (23)$$

$\overrightarrow{\vartheta_r} = Relative\ Velocity$

$\vec{\omega} = Rotational\ Velocity = 2.22\ rad/s$

$\bar{\tau_r} = Torque$

$\mathrm{P} = \mathrm{Pressure}$

$\bar{\vec{r}} = Rotor\ Radius = 7500 + 393.024 = 7893.024\ mm$

$\rho = Density\ of\ Flow = 1.225\ kg/m^3$

### 2.) Hand Calculations

The velocity on the blade can be calculated as follows ;

$$\overrightarrow{\vartheta_r} = r * \vec{\omega} \quad (24)$$

$$\overrightarrow{\vartheta_r} = r * \vec{\omega} \ = 2.22 \frac{rad}{s} * 7.893\ m = 17.52\ m/s$$

Betz Limit (Power Coefficient);

$$C_p = \frac{P_r}{0.5 * \rho * A * V_1^3} = \frac{P_r}{0.5 * \rho * \pi * \frac{D^2}{4} * V_1^3} = \frac{8\ kw}{0.5 * 1.225\pi * \left(\frac{7.893^2}{4}\right) * 5^3} = 0.21 = \%21 \quad (25)$$

In the results obtained from the simulation section, we will verify and compare these values.

## 3.5) Flow Analysis Results

After clicking on geometry in the results section, typing 3 in the Number of graphical instances section and clicking apply, all turbine blades were copied.

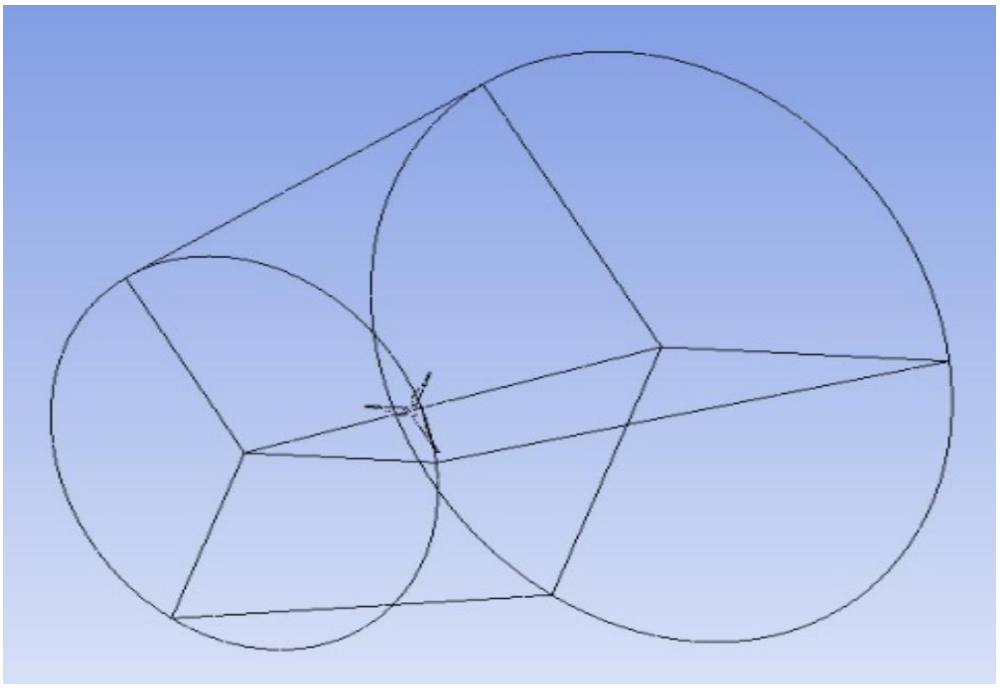

*Figure 36 Turbine Blades*

### 3.5.1) Static Pressure Contours

As a result of the flow analysis, we found the static pressure contours on blade as follows:

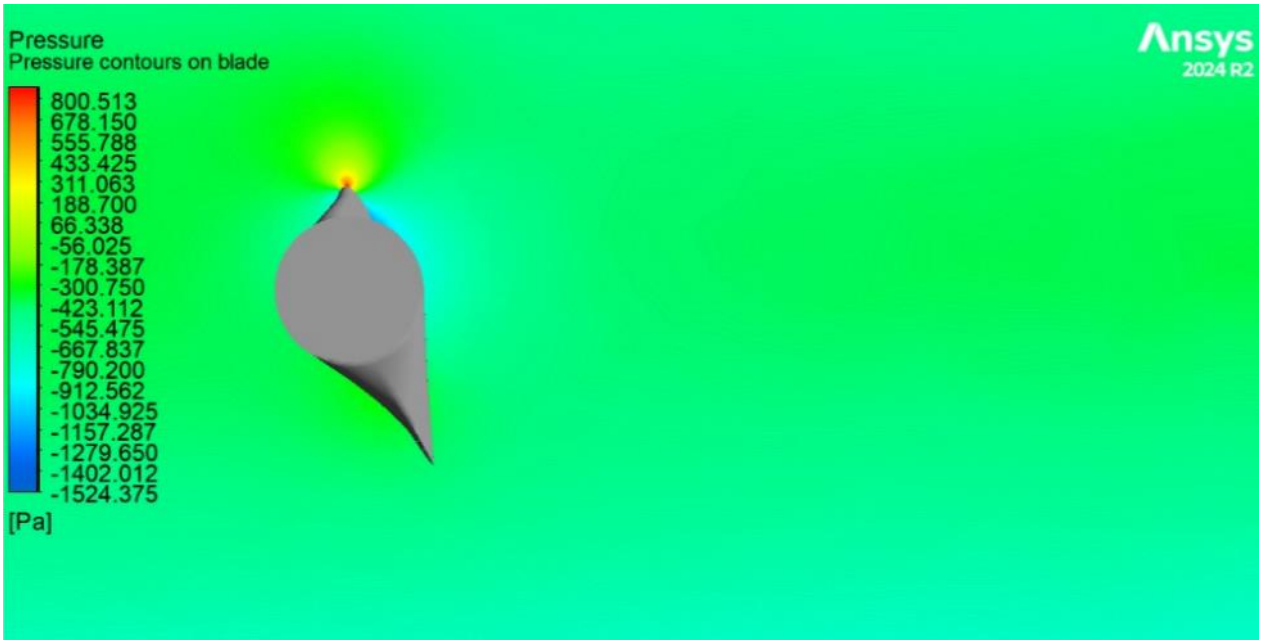


*Figure 37 Pressure Contours on Blade from side view*

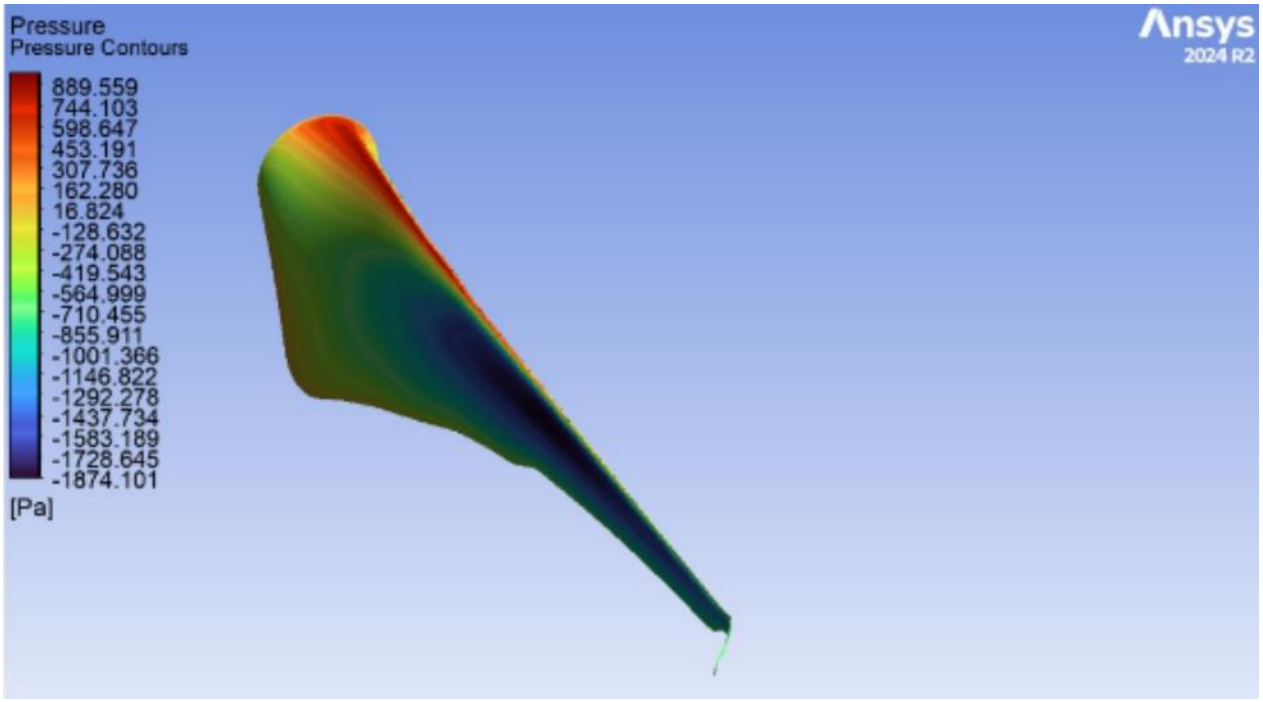


*Figure 38 Pressure Countur top view*

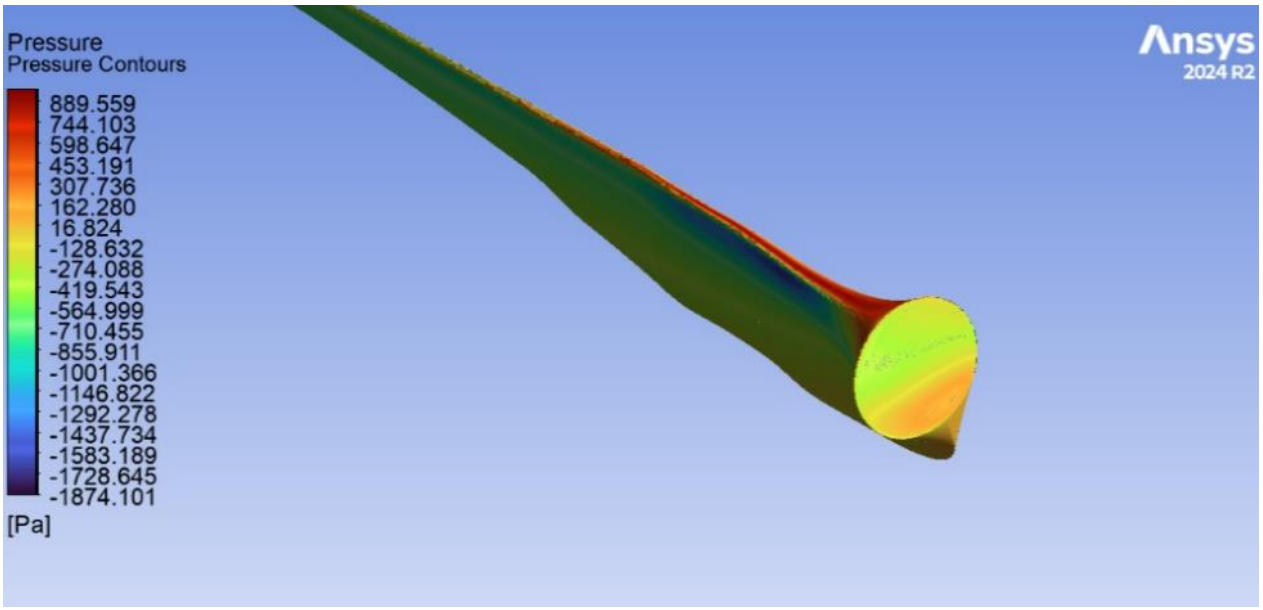


*Figure 39 Pressure Contour section view*

The incoming wind first impacts the leading edge, generating a high-pressure region. At the stagnation point, located at the blade tip, high pressure is observed due to the velocity being zero. On the upper surfaces of the blades, the fluid accelerates, leading to the formation of low-pressure regions. Conversely, the lower surfaces experience high-pressure regions due to the reduced velocity. As the angle of attack increases, the pressure on the upper surface decreases further, while the lower surface experiences an increase in pressure.

## 3.5.2) Velocity Contours

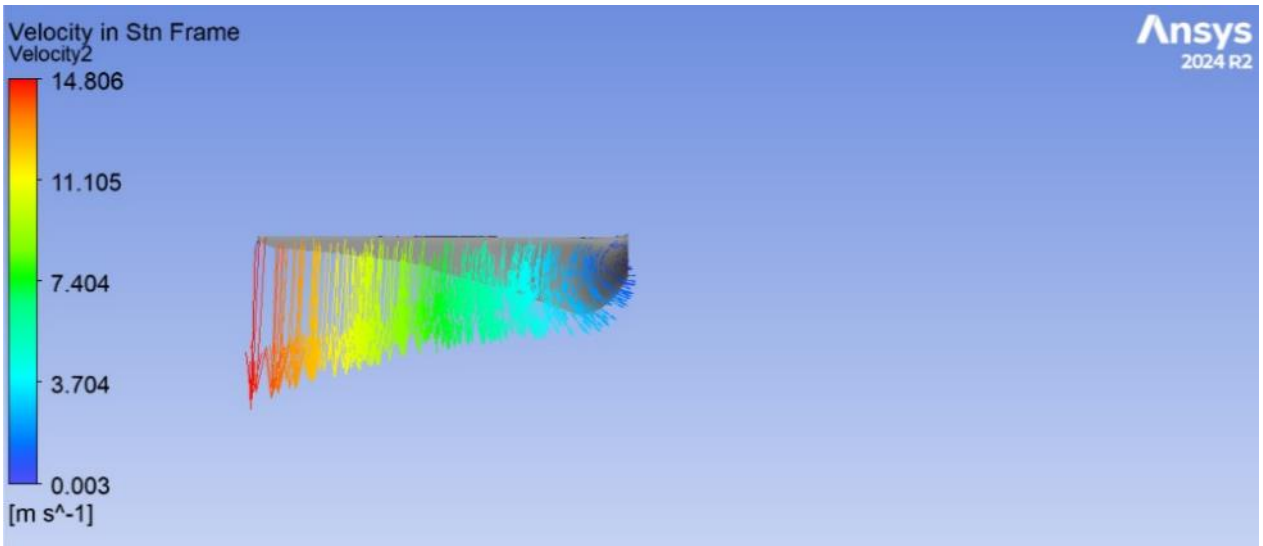


*Figure 40 Velocity Contour of Blade*

We calculated before

$$\overrightarrow{\vartheta_r} = r * \vec{\omega} = 2.22 \frac{rad}{s} * 7.893\, m = 17.52\, m/s$$

In ANSYS FLUENT results,

$$\overrightarrow{\vartheta_r} = 14.806\, m/s$$

Thus, we compared results.

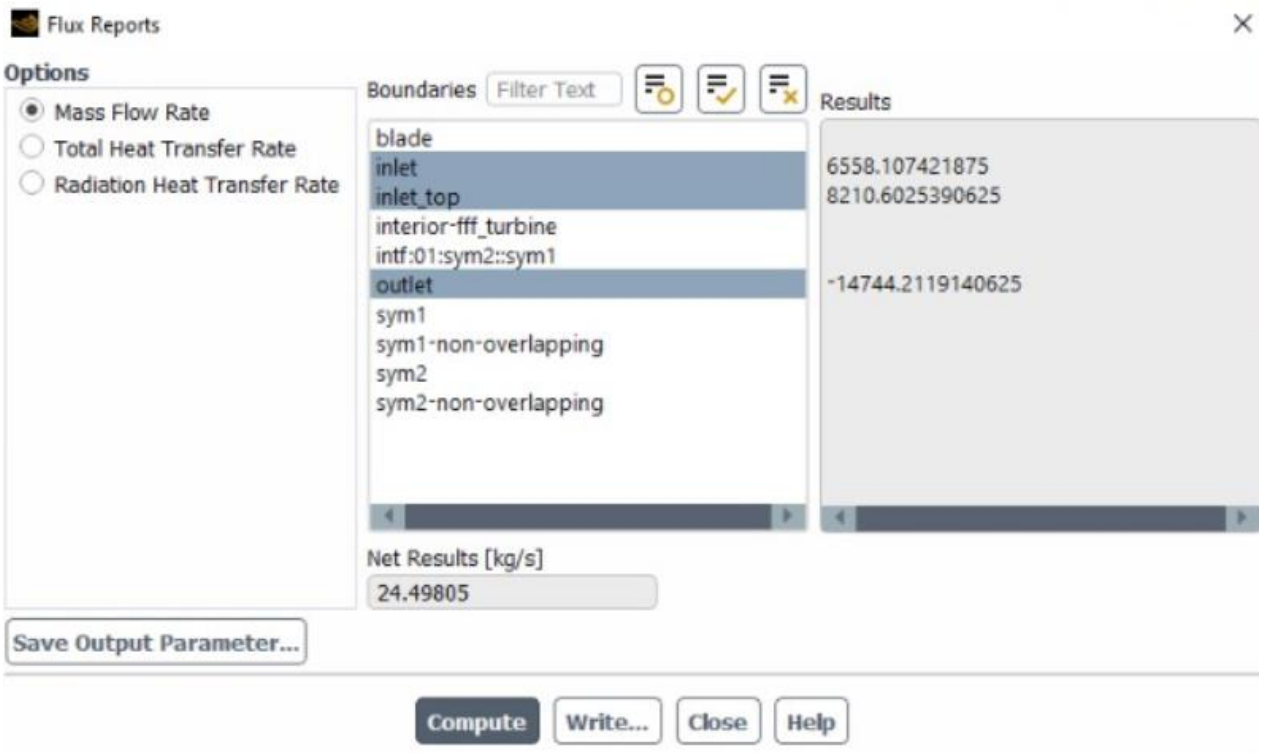


*Figure 41 Contiunitiy Equation Report*

To calculate Turbine Power $P_r$;

$$P_r = 0.5 * \rho * A * V_1^3 * Cp \tag{26}$$

It is possible to calculate Cp according to axial momentum theory.

According to momentum theory;

$$P_r = \beta * \bar{\tau_r} * \omega \tag{27}$$

$$\beta = Number\ of\ Turbnie\ Blade = 3$$

$$\omega = 2.22\ rad/s$$

$$\tau_r = Torque = 114.49\ Nm$$

(There is a - sign for the Z axis to rotate in the opposite negative direction.)

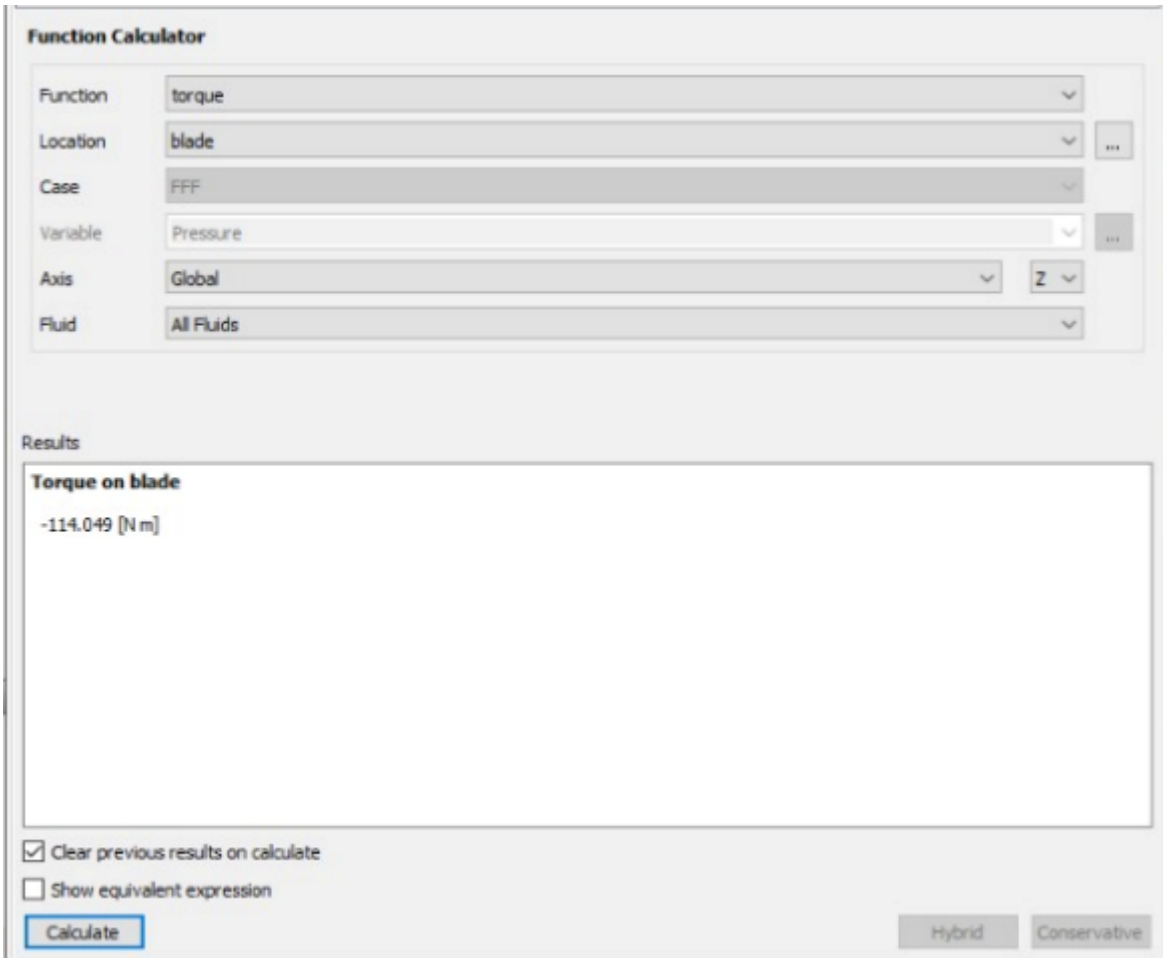


*Figure 42 Torque Value*

$$P_r = 762.95\ W$$

Calculated.

We calculate Cp from this turbine value.

$$C_P = 0.204 = \%20.4$$

It is very close to the value in the preliminary analysis of 21 percent.

### 3.5.6) Optimization

A completely modeled product can undergo digital examination and optimization procedures utilizing ANSYS and other simulation tools prior to actual manufacturing. With the use of these procedures, businesses may create new goods quickly and cheaply. The ANSYS software utilized in this work can conduct analysis and design optimization in a number of domains, such as electromagnetic, thermal, dynamic, static, and harmonic simulations. As a result, this software can be used to identify the design requirements needed to produce a high-quality product at a low cost.

Improving a product's material weight is one of the most prevalent optimization problems. Lower production costs are achieved by lighter products, yet manufacturers strive to maintain quality. They therefore put their designs through stringent optimization procedures during the new product development stage.

Even slight changes in the price of raw materials can have a big effect on manufacturing costs and, in turn, the final product's selling price in mass production. Businesses might increase their market share when production costs are reduced since the selling price becomes more competitive. They are therefore able to produce and release competitive goods onto the market.

ANSYS will be used in this study to examine and optimize the turbine's efficiency. The optimization procedure will concentrate on identifying the ideal blade angle of attack and limiting the rotational speed ($\omega$), as the highest efficiency that can be achieved for a turbine is 0.59.

Table of Schematic B2: Optimization

| | A | B | C | D |
|---|---|---|---|---|
| 1 | ⊟ Optimization Study | | | |
| 2 | Maximize P9 | Goal, Maximize P9 (Default importance) | | |
| 3 | ⊟ Optimization Method | | | |
| 4 | Adaptive Single-Objective | The Adaptive Single-Objective method is a gradient-based algorithm to provide a refined, global, optimization result. It supports a single objective, multiple constraints and aims at finding the global optimum. It is limited to continuous and manufacturable input parameters. | | |
| 5 | Configuration | Find 3 candidates in a maximum of 22 evaluations and 20 domain reductions. | | |
| 6 | Status | Converged after 22 evaluations. | | |
| 7 | ⊟ Candidate Points | | | |
| 8 | | Candidate Point 1 | Candidate Point 2 | Candidate Point 3 |
| 9 | P1 - AoT (degree) | 5 | 10 | 14,6 |
| 10 | P9 - cl_cd | 46,711 | 43,589 | 33,512 |

*Figure 43 P9 -cl/cd Parameter Optimization 1*

| Table of Schematic B2: Optimization | | | | |
|---|---|---|---|---|
| | A | B | C | D |
| 1 | Optimization Study | | | |
| 2 | Maximize P9 | Goal, Maximize P9 (Higher importance) | | |
| 3 | Optimization Method | | | |
| 4 | MOGA | The MOGA method (Multi-Objective Genetic Algorithm) is a variant of the popular NSGA-II (Non-dominated Sorted Genetic Algorithm-II) based on controlled elitism concepts. It supports multiple objectives and constraints and aims at finding the global optimum. | | |
| 5 | Configuration | Generate 10 samples initially, 10 samples per iteration and find 3 candidates in a maximum of 20 iterations. | | |
| 6 | Status | Converged after 36 evaluations. | | |
| 7 | Candidate Points | | | |
| 8 | | Candidate Point 1 | Candidate Point 2 | Candidate Point 3 |
| 9 | P1 - AoT (degree) | 7,5037 | 7,292 | 7,292 |
| 10 | P9 - Cl_Cd | 43,482 | 41,543 | 41,543 |

*Figure 44 Cl/Cd parameter optimization 2*

In this study, optimization was performed on a biomimetic wind turbine blade to enhance its performance by analyzing different angles of attack (AoT) and the P9 - $c_l/c_d$ parameter. Using ANSYS software, both the **Adaptive Single-Objective** and **MOGA (Multi-Objective Genetic Algorithm)** optimization methods were applied, and the top three candidates for each method were determined.

In the **Adaptive Single-Objective** optimization, the best-performing three candidates had P9 - $c_l/c_d$ values of **46.711**, **43.589**, and **33.512**, with corresponding angles of attack found to be **10°** and **14.6°**.

For the **MOGA** optimization method, the three selected candidates had P9 - $C_l/C_d$ values of **43.482**, **41.543**, and **41.543**, with optimized angles of attack measured at **7.5037°**, **7.292°**, and **7.292°**.

| Table of Schematic B2: Optimization | | | | |
|---|---|---|---|---|
| | A | B | C | D |
| 1 | Optimization Study | | | |
| 2 | Maximize P9 | Goal, Maximize P9 (Default importance) | | |
| 3 | Optimization Method | | | |
| 4 | Adaptive Single-Objective | The Adaptive Single-Objective method is a gradient-based algorithm to provide a refined, global, optimization result. It supports a single objective, multiple constraints and aims at finding the global optimum. It is limited to continuous and manufacturable input parameters. | | |
| 5 | Configuration | Find 3 candidates in a maximum of 22 evaluations and 20 domain reductions. | | |
| 6 | Status | Not Converged because the Maximum Number of Evaluation is reached . | | |
| 7 | Candidate Points | | | |
| 8 | | Candidate Point 1 | Candidate Point 2 | Candidate Point 3 |
| 9 | P1 - AoT (degree) | 3,7276 | 8,1569 | 10,978 |
| 10 | P9 - cl_cd | 44,664 | 44,469 | 42,831 |

*Figure 45 cl/cd parameter optimization 3*

In this optimization study, the **Adaptive Single-Objective** method was used to maximize P9 - $c_l/c_d$. The optimization process involved **22 evaluations**, but the process did not converge as it reached the maximum number of evaluations. The top three candidate points were identified with **P9** - $c_l/c_d$ values of **44.664**, **44.469**, and **42.831**, corresponding to angles of attack (AoT) of **3.7276°**, **8.1569°**, and **10.978°**.

| Table of Schematic B2: Optimization | | | | |
|---|---|---|---|---|
| | A | B | C | D |
| 1 | Optimization Study | | | |
| 2 | Maximize P9 | Goal, Maximize P9 (Higher importance) | | |
| 3 | Optimization Method | | | |
| 4 | MOGA | The MOGA method (Multi-Objective Genetic Algorithm) is a variant of the popular NSGA-II (Non-dominated Sorted Genetic Algorithm-II) based on controlled elitism concepts. It supports multiple objectives and constraints and aims at finding the global optimum. | | |
| 5 | Configuration | Generate 10 samples initially, 10 samples per iteration and find 3 candidates in a maximum of 20 iterations. | | |
| 6 | Status | Converged after 36 evaluations. | | |
| 7 | Candidate Points | | | |
| 8 | | Candidate Point 1 | Candidate Point 2 | Candidate Point 3 |
| 9 | P1 - AoT (degree) | 7,5037 | 7,292 | 7,3033 |
| 10 | P9 - Cl_Cd | 42,638 | 41,944 | 40,958 |

*Figure 46 Cl/Cd Parameter Optimization 4*

The **MOGA** method was applied to maximize P9 - $C_l\ /C_d$, with a **higher importance** assigned to the objective. The optimization process involved **36 evaluations**, successfully converging. The top three candidates had **P9 -** $C_l\ /C_d$ values of **42.638**, **41.994**, and **40.958**, with their corresponding angles of attack at **7.5037°**, **7.292°**, and **7.3033°**.

Table of Schematic B2: Optimization

| | A | B | C | D |
|---|---|---|---|---|
| 1 | Optimization Study | | | |
| 2 | Maximize P9 | Goal, Maximize P9 (Default importance) | | |
| 3 | Optimization Method | | | |
| 4 | Adaptive Multiple-Objective | The Adaptive Multiple-Objective method is a variant of the popular NSGA-II (Non-dominated Sorted Genetic Algorithm-II) based on controlled elitism concepts. It supports multiple objectives and constraints and aims at finding the global optimum. It is limited to continuous and manufacturable input parameters. | | |
| 5 | Configuration | Generate 100 samples initially, 50 samples per iteration and find 3 candidates in a maximum of 20 iterations. | | |
| 6 | Status | Converged after 264 evaluations. | | |
| 7 | Candidate Points | | | |
| 8 | | Candidate Point 1 | Candidate Point 2 | Candidate Point 3 |
| 9 | P1 - AoT (degree) | 5,5662 | 4,8061 | 4,9081 |
| 10 | P9 - Cl_Cd | 44,408 | 44,16 | 43,368 |

*Figure 47 Cl/Cd parameter Optimization 5*

In the third study, the **Adaptive Multiple-Objective** optimization method was implemented, allowing multiple constraints and objectives while maximizing P9 - $C_l\ /C_d$. This method involved **264 evaluations**, successfully converging after extensive iterations. The top three optimized candidates had **P9 -** $C_l\ /C_d$values of **44.408**, **44.16**, and **43.368**, with angles of attack found to be **5.5662°**, **4.8061°**, and **4.9081°**.

Table of Schematic B2: Optimization

| | A | B | C | D |
|---|---|---|---|---|
| 1 | Optimization Study | | | |
| 2 | Maximize P4 | Goal, Maximize P4 (Default importance) | | |
| 3 | Seek P8 = 0,59 kg s^-3 radian | Goal, Seek P8 = 0,59 kg s^-3 radian (Default Importance) | | |
| 4 | Optimization Method | | | |
| 5 | Adaptive Multiple-Objective | The Adaptive Multiple-Objective method is a variant of the popular NSGA-II (Non-dominated Sorted Genetic Algorithm-II) based on controlled elitism concepts. It supports multiple objectives and constraints and aims at finding the global optimum. It is limited to continuous and manufacturable input parameters. | | |
| 6 | Configuration | Generate 8 samples initially, 8 samples per iteration and find 3 candidates in a maximum of 7 iterations. | | |
| 7 | Status | Converged after 25 evaluations. | | |
| 8 | Candidate Points | | | |
| 9 | | Candidate Point 1 | Candidate Point 2 | Candidate Point 3 |
| 10 | P1 - AoA (degree) | 84,386 | 83,816 | 84,375 |
| 11 | P4 - cl_cd-op | 58,312 | 59,601 | 59,876 |
| 12 | P8 - Cp (kg s^-3 radian) | 0,37213 | 0,3718 | 0,3655 |

*Figure 48 Maximizing Cl/Cd Values*

To find the ideal angle of attack (AoA) for optimizing the lift-to-drag ratio (Cl/Cd), the optimization procedure was carried out in the Figure 47. According to the results, the highest Cl/Cd value was discovered at an AoA of 84.386°, as indicated in the table. The blade achieves the maximum lift and the least amount of drag at this angle because it offers the best aerodynamic efficiency.

Table of Schematic D2: Optimization

| | T | U | V | W | X | Y | Z | AA | AB | AC | AD | AE | AF |
|---|---|---|---|---|---|---|---|---|---|---|---|---|---|
| 1 | Factor Minimum | P69 - Cl/Cd | P70 - cord1 | P71 - cord2 | P72 - cord3 | P73 - cord4 | P74 - cord5 | P75 - cord6 | P76 - cord7 | P77 - cord8 | P78 - Average cord | P80 - A | P81 - indicated drag (kg^2 m^2 s^-4) |
| 68 | | | | | | | | | | | | | |
| 69 | | | | | | | | | | | | | |
| 70 | | | | | | | | | | | | | |
| 71 | | 4,7683 | 205,89 | 182,21 | 173,96 | 117,65 | 75,839 | 57,098 | 28,033 | 9,762 | 106,3 | 3,6972 | 0,018004 |
| 72 | | | | | | | | | | | | | |
| 73 | | | | | | | | | | | | | |
| 74 | | 4,4349 | 205,89 | 184,99 | 124,32 | 117,65 | 64,946 | 46,51 | 19,929 | 11,767 | 97,001 | 4,0518 | 0,010847 |
| 75 | | 5,0095 | 205,89 | 185,92 | 168,44 | 117,65 | 84,554 | 52,392 | 22,03 | 12,436 | 106,16 | 3,702 | 0,018296 |
| 76 | | | | | | | | | | | | | |
| 77 | | 5,182 | 205,89 | 187,78 | 190,5 | 117,65 | 71,482 | 30,274 | 26,232 | 13,773 | 105,45 | 3,7272 | 0,020497 |
| 78 | | | | | | | | | | | | | |
| 79 | | | | | | | | | | | | | |
| 80 | | | | | | | | | | | | | |
| 81 | | | | | | | | | | | | | |

Chart: No data

*Figure 49 Optimization Results*

The values derived from the optimum setup (84.386° AoA) are shown in Row 74 of the Figure 48, which displays the results of static analysis. This row contains a number of aerodynamic variables, including chord lengths, pressure distributions, indicated drag values, and the lift-to-

drag ratio (P9-Cl/Cd). These numbers are essential for confirming the enhanced blade design's stability and efficiency.

These outcomes support the optimization study's conclusions by demonstrating that the optimal angle (84.386°) produces the most aerodynamically efficient blade performance.

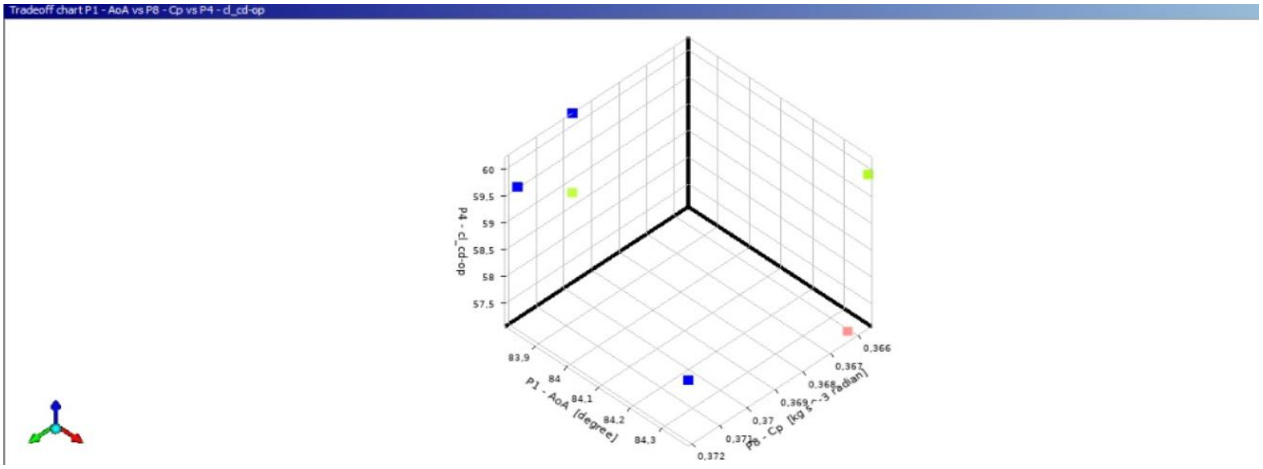


*Figure 50 AoA vs P8 - Cp vs P4 - cl_cd-op*

# 4.) RESULTS AND DISCUSSION

This project focuses on a **biomimetic wind turbine blade**. Initially, a preliminary analysis was conducted to determine the methodology for calculating the energy output of a **three-bladed wind turbine**, with the relevant formulas outlined in detail. These formulas were then used to generate diagrams illustrating the relationship between power/torque and various factors such as **blade design, wind angle of attack, and rotational speed**.

To validate the theoretical calculations, simulations were carried out using the **FLUENT module in ANSYS WORKBENCH**, ensuring that the obtained results aligned with theoretical expectations. Additionally, the wind turbine blade and **biomimetic winglet** were optimized within the software, and the findings from this optimization were documented in the report.

In this study, the wind speed was assumed to be constant. However, in real-world conditions, wind speed fluctuates. Sudden changes in wind velocity can induce stress on the blades, making it essential to verify the calculated blade dimensions against the **maximum wind speeds** expected in the target region.

**For 1000 mm**

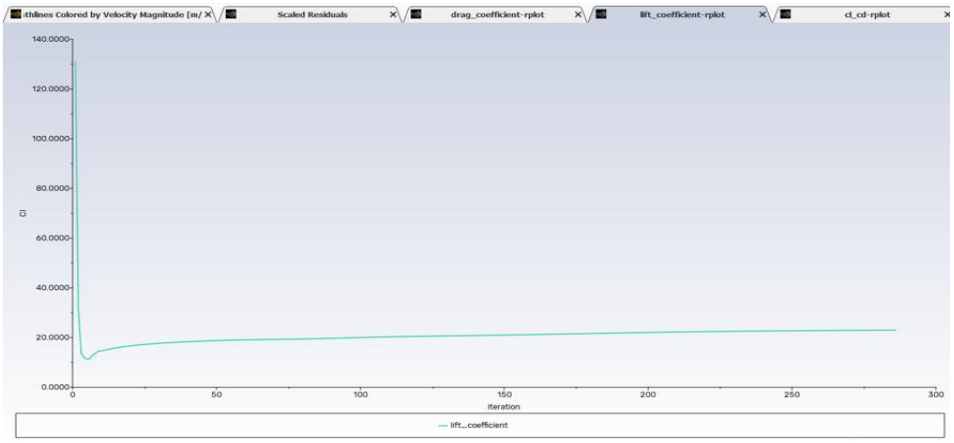


*Figure 51 Lift Coefficient Graph*

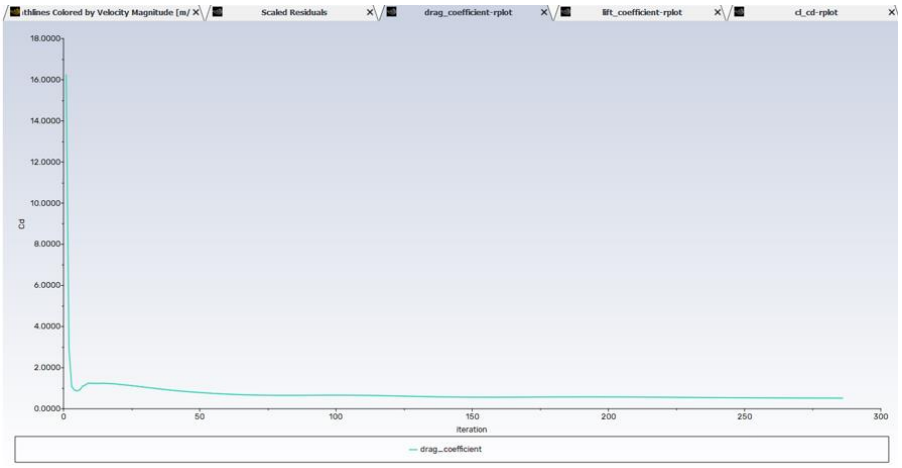


*Figure 52 Drag Coefficient Graph*

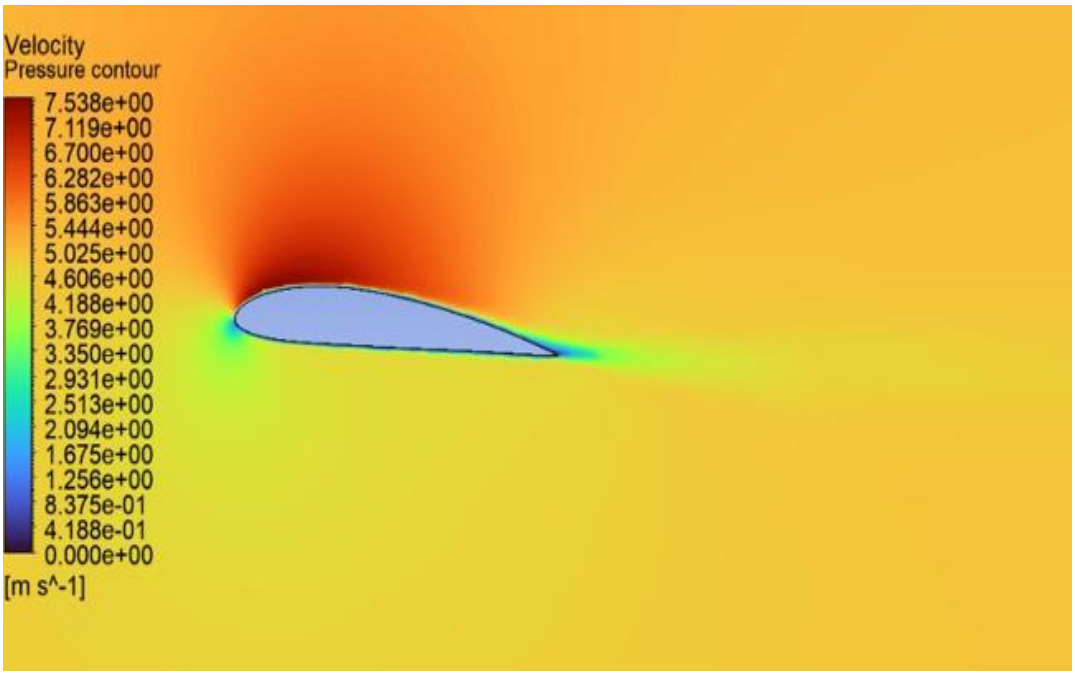


*Figure 53 Velocity distribution analysis around the airfoil*

**For 1100 mm**

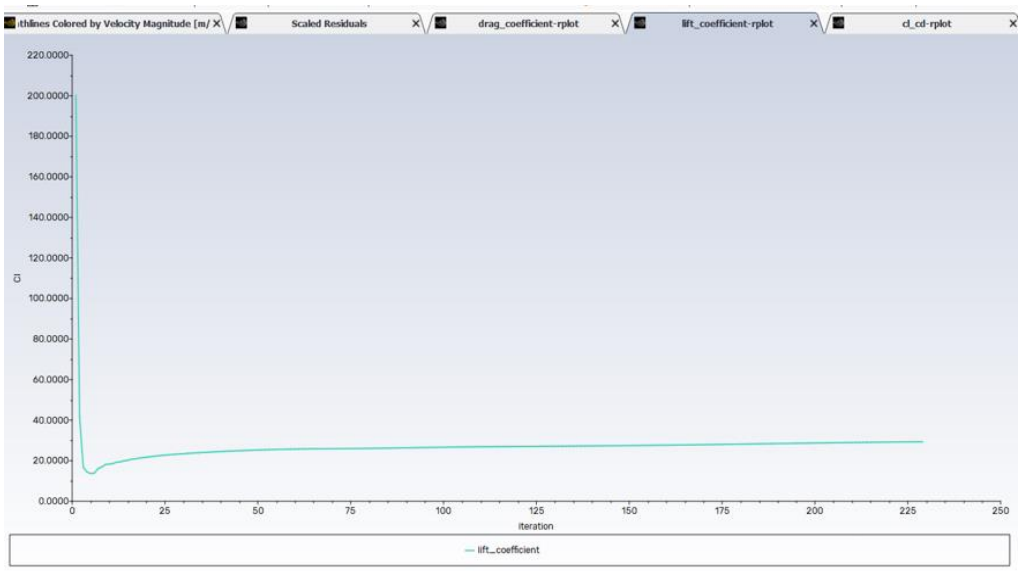


*Figure 54 Lift Coefficient*

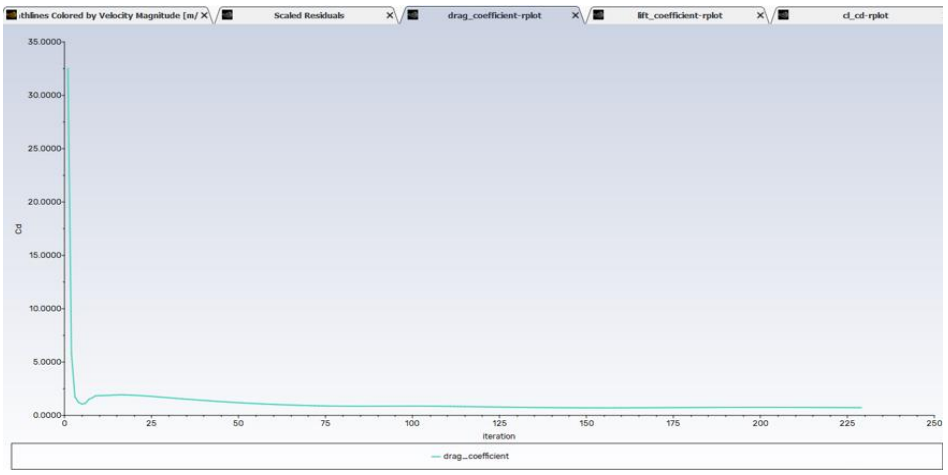


*Figure 55 Drag Coefficient*

## For 1100 mm

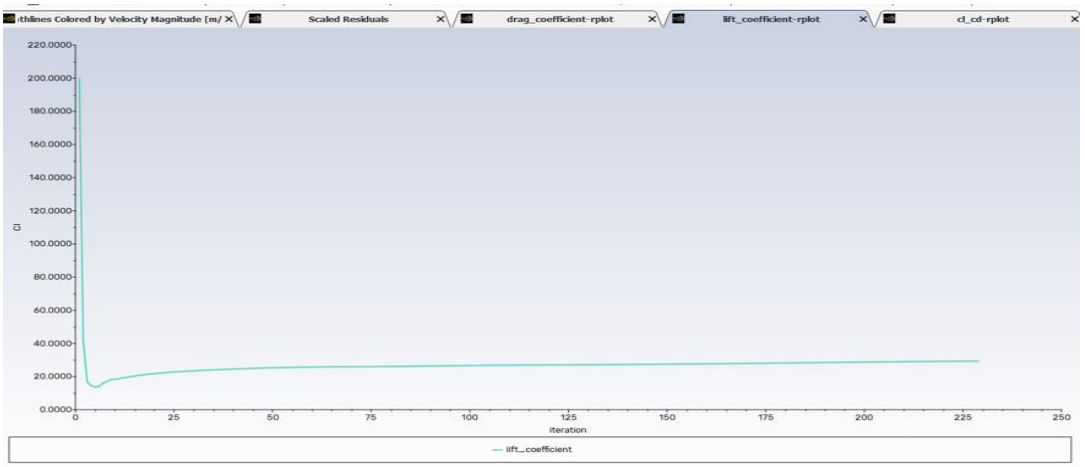


*Figure 56 Lift Coefficient*

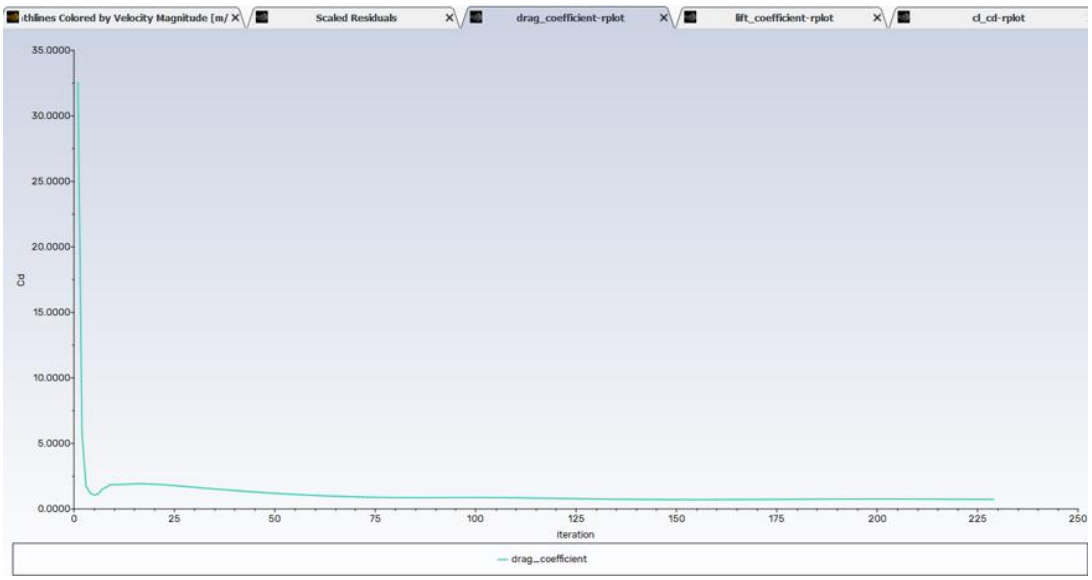


*Figure 57 Drag Coefficient*

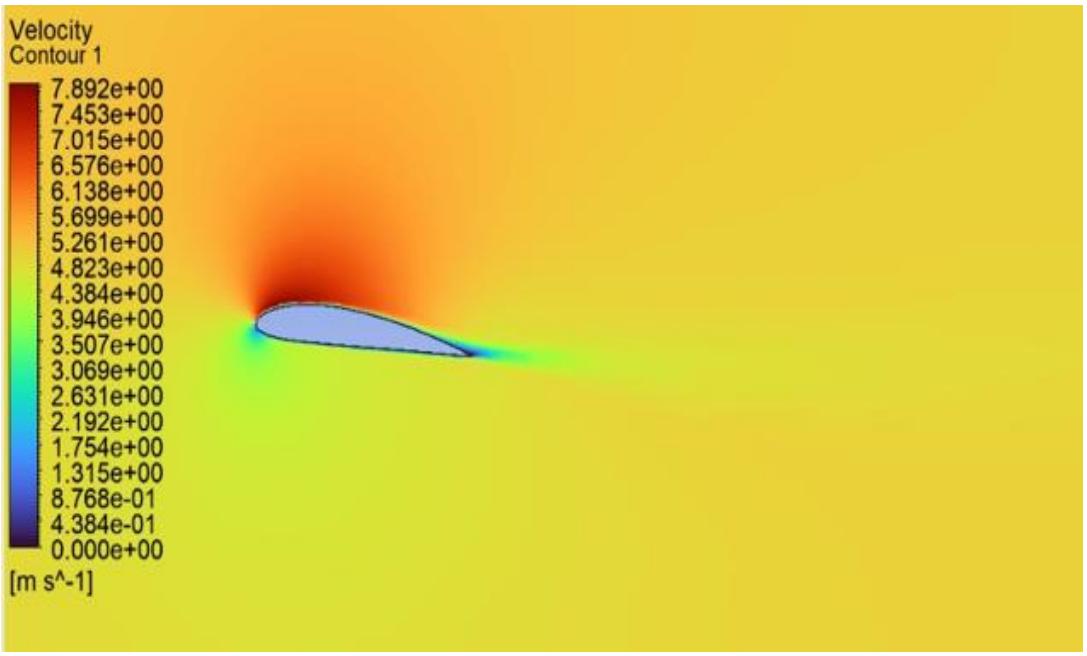


*Figure 58 Velocity distribution analysis around the airfoil*

**For 1210 mm**

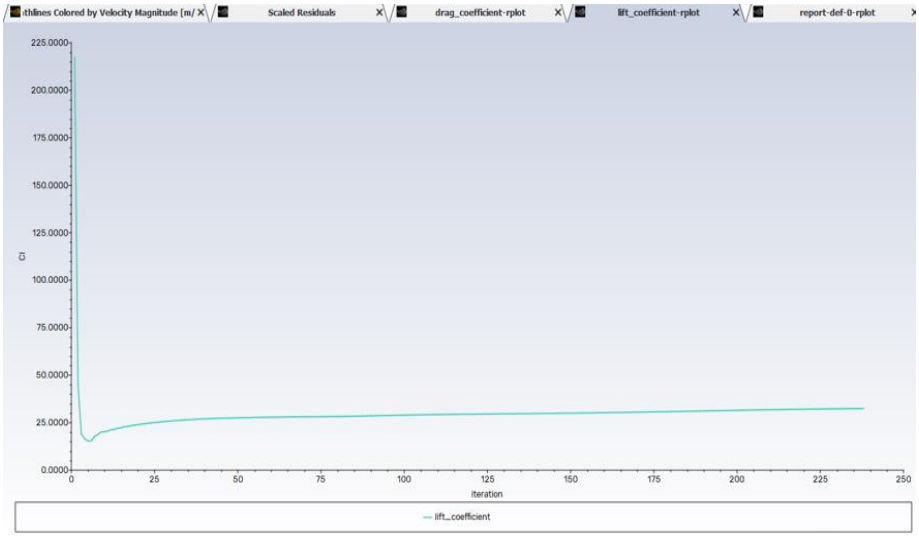


*Figure 59 Lift Coefficient Graph*

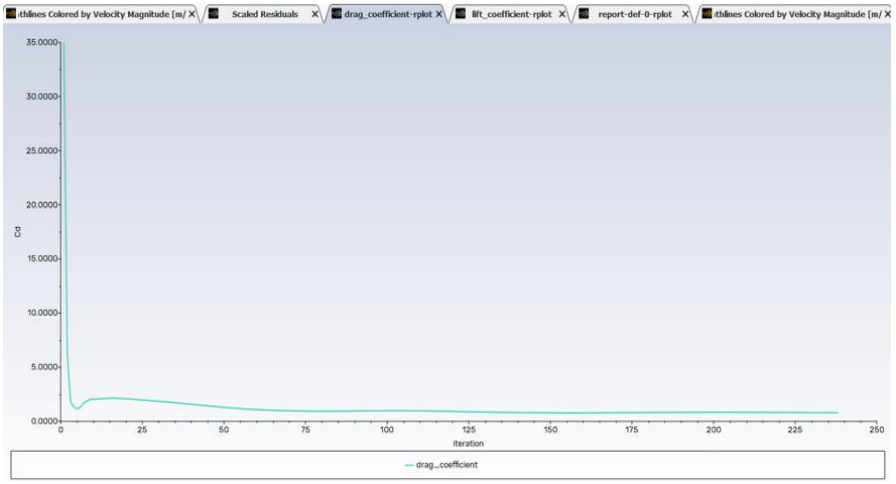


*Figure 60 Drag Coefficient Graph*

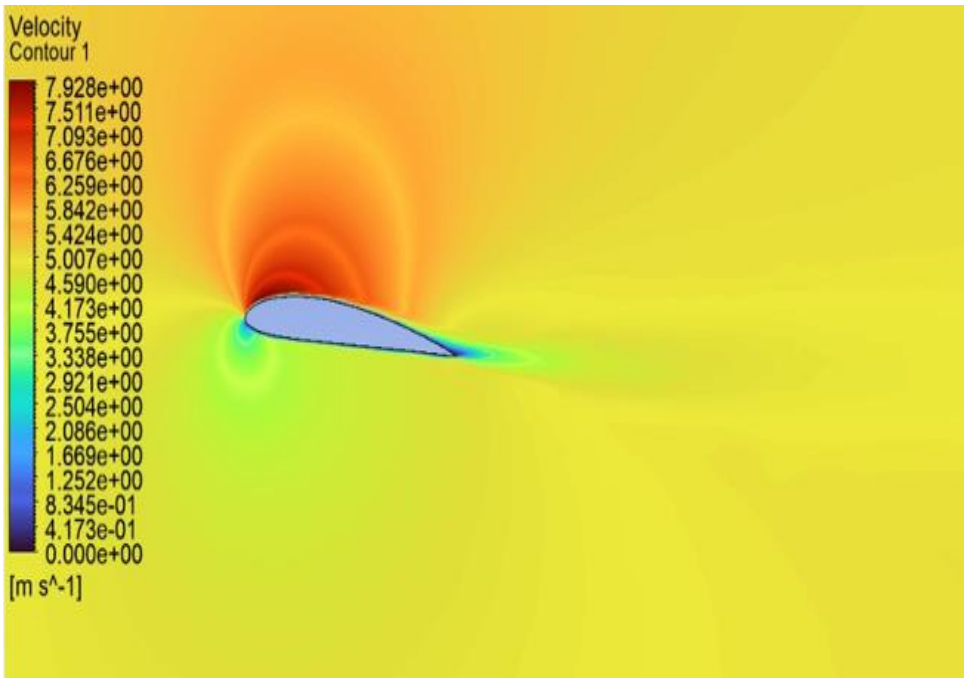


*Figure 61 Velocity distribution analysis around the airfoil*

**For 1331 mm**

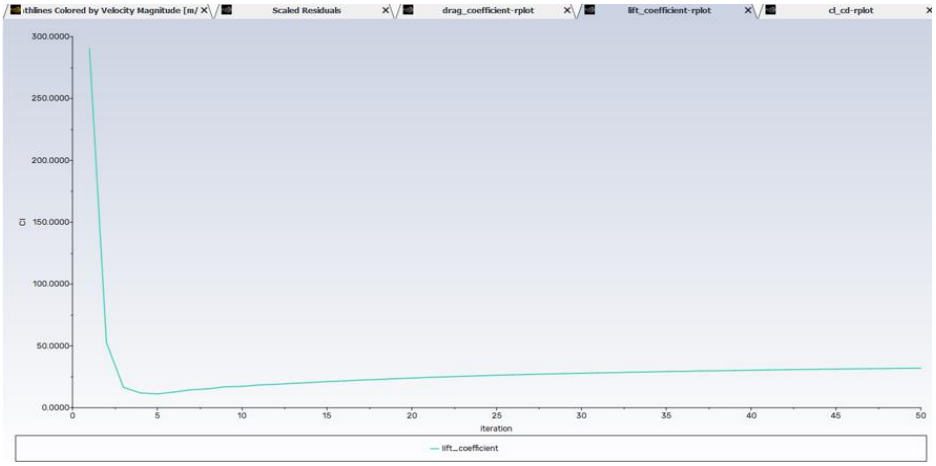


*Figure 62 Lift Coefficient Graph*

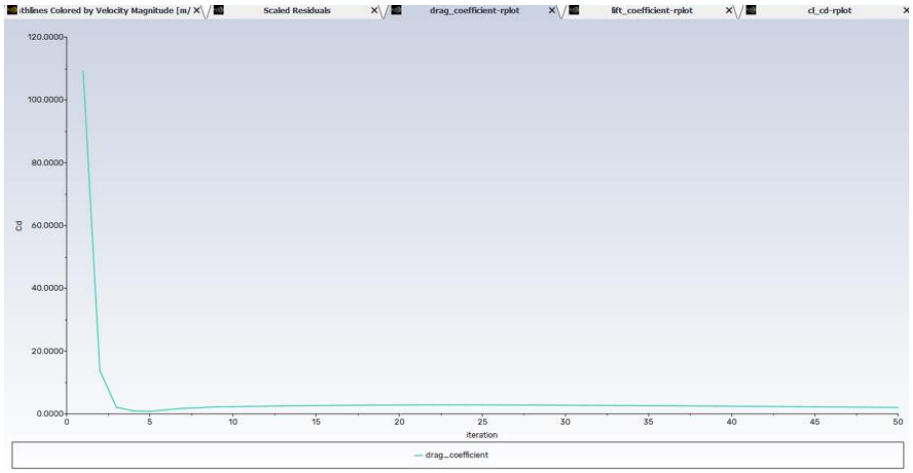


*Figure 63 Drag Coefficient Graph*

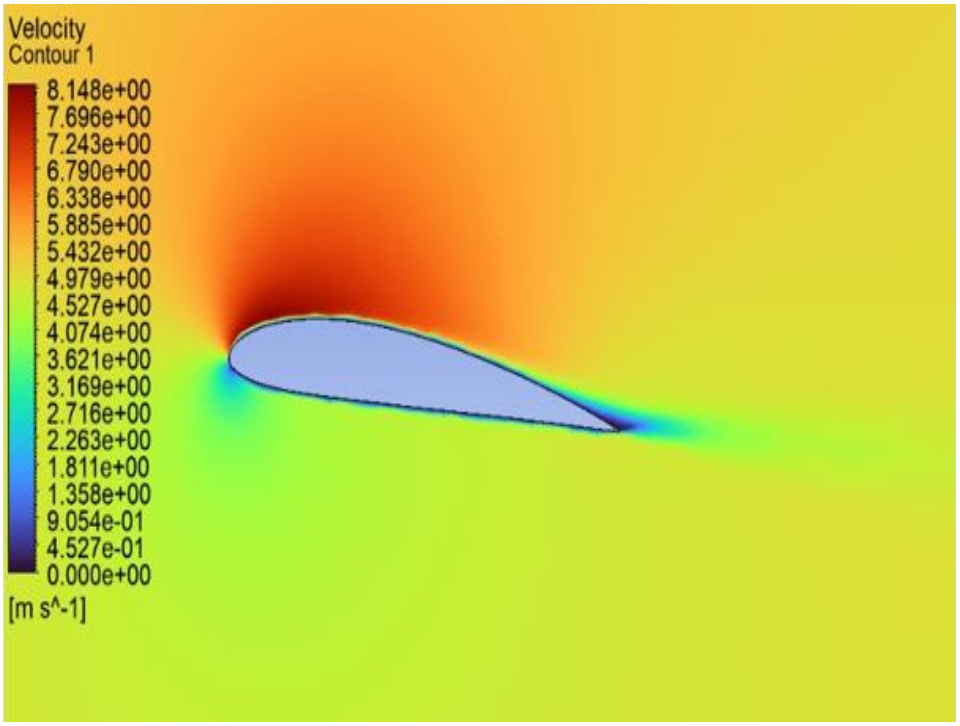


*Figure 64 Velocity distribution analysis around the airfoil*

**For 1464.1 mm**

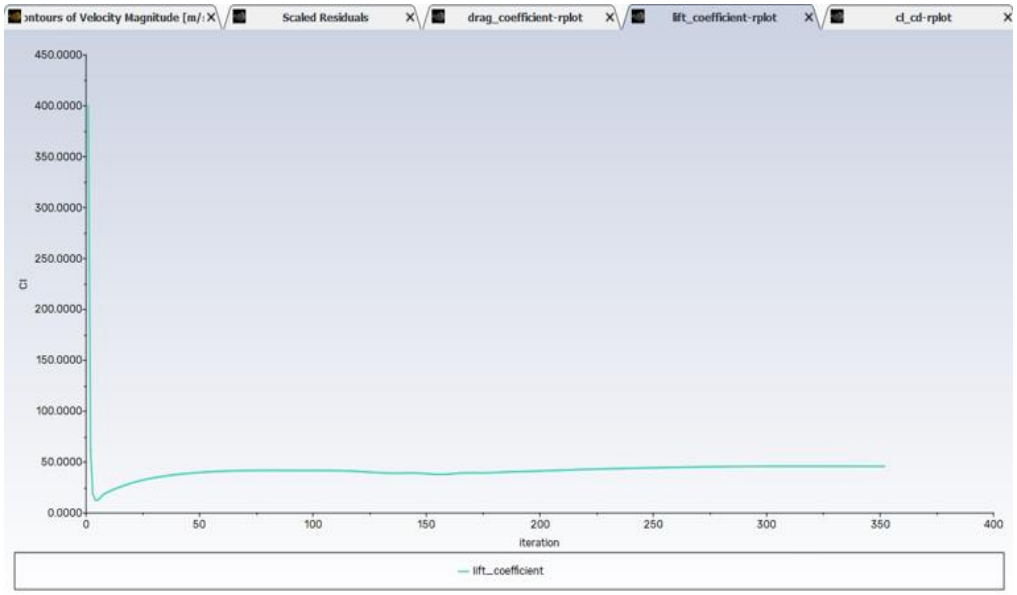


*Figure 65 Lift Coefficient Graph*

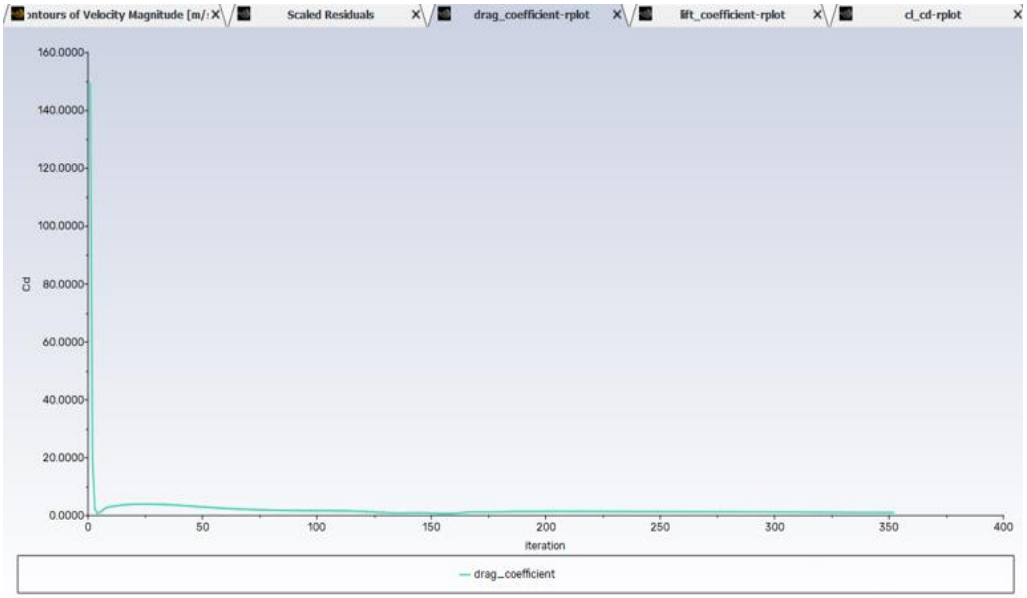


*Figure 66 Drag Coefficient Graph*

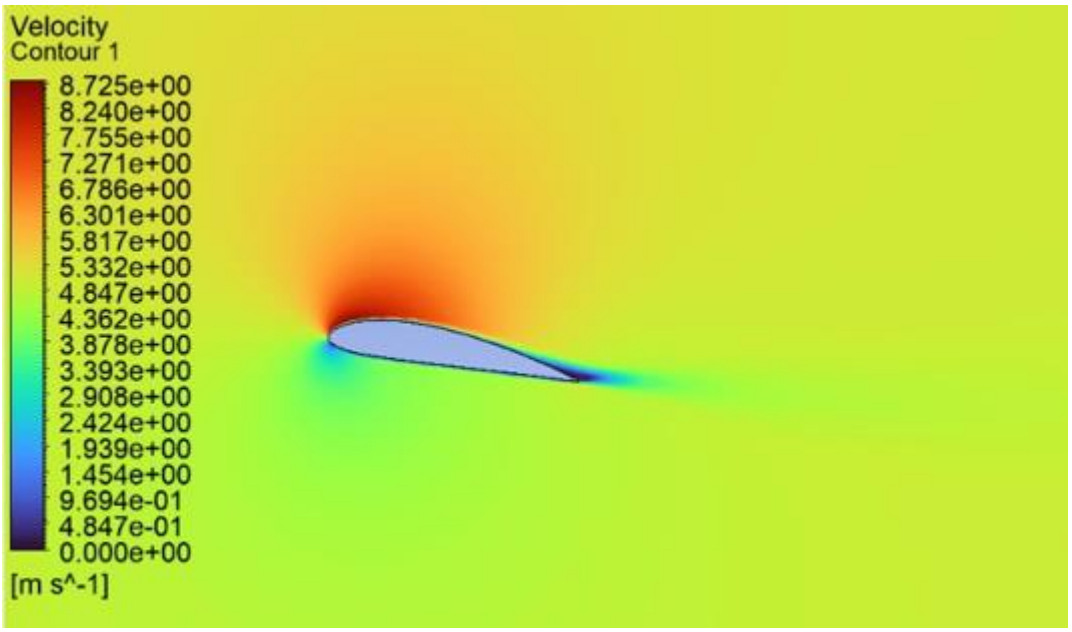


*Figure 67 Velocity distribution analysis around the airfoil*

## 4.1) Manufacturability and Cost Analysis of the Biomimetic Wind Turbine Blade with Winglet

### 4.1.1) Manufacturability Analysis

**Material Selection and Processability**

- **Blade Material:** Carbon Fiber Reinforced Polymer (CFRP) has been selected due to its **high strength-to-weight ratio**, which enhances aerodynamic efficiency while minimizing structural loads. However, its production requires **special molding and resin infusion techniques**.

- **Winglet Material**: The same composite material can be used for the winglet. To ensure high stress and vibration resistance, a layered composite structure is recommended.

**Manufacturing Methods**

- **RTM (Resin Transfer Molding):** Suitable for medium to large-scale production, but **initial mold costs are high**.

- **Vacuum Infusion:** More cost-effective but requires longer processing times.

- **Autoclave Method:** Provides the highest strength but **requires high-temperature and high-pressure curing**, making it expensive.

**Manufacturing Challenges**

- **Blade Size:** At 6.6 meters, a **large mold and curing oven** are necessary.

- **Twist Angle:** The varying twist along the blade could **complicate fabrication**, requiring **CNC cutting and customized molds**.

- **Winglet Integration:** The winglet section **requires layered composite layups**. It can either be **manufactured separately and assembled later** or **produced as an integrated part of the blade**.

## 4.1.2) Cost Analysis

*Table 4 Raw Materials Cost*

| Material | Average Price ($/kg) | Estimated Quantity | Total Cost ($) |
|---|---|---|---|
| CFRP (Prepreg) | 40 – 60 | ~100 kg | 4000 - 6000 |
| Epoxy Resin | 10 - 20 | ~20 kg | 200 - 400 |
| Core Material (Honeycomb or Foam) | 50 - 80 | ~30 kg | 1500 - 2400 |
| Quality Control & Testing | - | - | 500 - 1000 |
| Labor & Manufacturing | - | - | 2000 - 5000 |
| Total Cost | - | - | $8200 - $14,800 |

**Note:** Prices are estimated based on market averages. Costs may decrease with higher production volumes.

**Manufacturing & Assembly Costs**

- **Mold Production:** One of the **most significant initial costs**, ranging from **$10,000 to $20,000**.
- **Labor & Machinery:** CNC cutting, manual layup, and autoclave processing could add **$2000 - $5000** in costs.
- **Assembly & Finishing:** Painting, aerodynamic surface finishing, and quality checks (~$500 - $1000).

### 4.1.3) Manufacturability Decision & Recommendations

**Manufacturable**: However, to make it cost-effective for mass production, optimizations in material usage and production techniques are needed.

**Recommended Manufacturing Method**: Vacuum infusion + post-curing in an oven (best balance between cost and performance).

**Challenges to Consider**:

- High initial investment is required for prototyping.
- Modular blade and winglet design could make maintenance and part replacement easier.
- CFRP waste management should be planned, as recycling is difficult.

# 5.) CONCLUSION

This study aimed to optimize a wind turbine blade using biomimetic principles inspired by the aerodynamics of vulture wings. The main objective was to improve aerodynamic efficiency by reducing induced drag and increasing the lift-to-drag ratio through the addition of a bio-inspired winglet.

A thorough analysis was performed using Computational Fluid Dynamics (CFD) and Finite Element Analysis (FEA) within ANSYS Fluent and Static Structural modules. Initially, the winglet material was Al 7075-T6, resulting in a Factor of Safety (FOS) of 15, indicating excessive structural strength and unnecessary weight. To refine the design, alternative materials such as Al 6061-T6 and Glass Fiber Reinforced Polymer (GFRP) were investigated, bringing the FOS down to an optimal range of 2-3 while preserving structural integrity.

The findings showed that biomimetic winglets significantly reduce induced drag, thereby enhancing wind turbine performance. The optimized design strikes a balance between mechanical strength and weight efficiency, making it suitable for practical applications. Future research could focus on further aerodynamic improvements, experimental validation, and integration with full-scale wind turbine systems.

In conclusion, this research emphasizes the potential of biomimetic principles in wind energy applications and highlights the importance of material and structural optimization to achieve both efficiency and sustainability.

# 6.) REFERENCES


- Metin U, Özdemir M, Yildirim ÇV, Çoban S. A novel biomimetic wing design and optimizing aerodynamic performance. J Aviat. 2022;6(1):12–3.

- Mitchell S, Ogbonna I, Volkov K. Improvement of self-starting capabilities of vertical axis wind turbines with new design of turbine blades. Sustain. 2021;13(7):3854–24.

- Zhao M, Cao H, Zhang M, Liao C, Zhou T. Optimal design of aeroacoustic airfoils with owl-inspired trailing-edge serrations. Bioinspir Biomim. 2021;16(5):056004–14.

- Hua X, Zhang C, Wei J, Hu X, Wei H. Wind turbine bionic blade design and performance analysis. J Vis Commun Image R. 2019;60(3):258–7

- Dai, Y., Wang, D., Liu, X., Wu, W. (2024). Optimized design of bio-inspired wind turbine blades. *Fluid Dynamics & Materials Processing*, *20(7)*, 1647–1664. https://doi.org/10.32604/fdmp.2024.046158

- Zhu J, Cai X, Gu R. Aerodynamic and structural integrated optimization design of horizontal-axis wind turbine blades. Energies. 2016;9(2):66.

- Zemamou M, Toumi A, Mrigua K, Lahlou Y, Aggour M. A novel blade design for Savonius wind turbine based on polynomial bezier curves for aerodynamic performance enhancement. Int J Green Energy. 2020;17(11):652–14

- Tang X, Huang X, Peng R, Liu X. A direct approach of design optimization for small horizontal axis wind turbine blades. Procedia CIRP. 2015;36(1):12–5.

- Zeisberger, V.M. Derive New Profile Shapes for Efficient Smal Urban Wind Turbines—A Biomimetic Approach. Master’ Thesis, University of Groningen, Groningen, The Netherlands, 2021

- Wei Zhong, Wen Zhong Shen 2,Tong Guang Wang and Wei Jun Zhu 2019 A New Method of Determination of the Angle of Attack on Rotating Wind Turbine Blades

- Qing'an Li, Jianzhong Xu, Yasunari Kamada, Maeda Takao, Shogo Nishimura,Guangxing Wu, Chang Cai 2019 Experimental investigations of airfoil surface flow of a horizontal

axis wind turbine with LDV measurements

- Mehmet Bakırcı, Sezayi Yılmaz 2018 Theoretical and computational investigations of the optimal tip-speed ratio of horizontal-axis wind turbines

- Lei Zhang, Xingxing Li, Shuang Li, Jingyan Bai, Jin Xu 2020 Unstable aerodynamic performance of a very thick wind turbine airfoil CAS-W1-450

- Basom, B. and Maughmer, M. D., "Inviscid Analysis of Horizontal-Axis Wind Turbines Using Distributed Vorticity Elements," 49th AIAA Aerospace Sciences Meeting and Exhibit, AIAA 2011-539, Orlando, FL, 2011

- Bramesfeld, G. and Maughmer, M. "Relaxed-Wake Vortex-Lattice Method Using Distributed Vorticity Elements." Journal of Aircraft, Vol. 45, No. 2, March-April 2008

- Johansen, J. and Sørensen, N., "Numerical Analysis of Winglets on Wind Turbine Blades using CFD," Risø, 2007. Paper 2007_126.

- Gaunaa, M. and Johansen, J., "Can CP be Increased by the Use of Winglets? – or – A Theoretical and Numerical Investigation of the Maximum Aerodynamic Efficiency of Wind Turbine Rotors with Winglets," AIAA, 2008. AIAA 2008-1314

- A numerical study of bio-inspired wingtip modifications of modern wind turbines Khashayar RahnamayBahambary ∗ , Mohammad Reza Kavian-Nezhad, Alexandra Komrakova, Brian A. Fleck

- Guerrero, Joel E., Dario Maestro, and Alessandro Bottaro. "Biomimetic spiroid winglets for lift and drag control." Comptes Rendus Mecanique 340, no. 1-2 (2012): 67-80